

Review

# Development of Thermochemical Heat Storage Based on CaO/CaCO<sub>3</sub> Cycles: A Review

Ying Yang, Yingjie Li \*, Xianyao Yan, Jianli Zhao \* and Chunxiao Zhang

Shandong Engineering Laboratory for High-Efficiency Energy Conservation and Energy Storage Technology & Equipment, School of Energy and Power Engineering, Shandong University, Jinan 250061, China; yangying03@mail.sdu.edu.cn (Y.Y.); yanxy1009@163.com (X.Y.); zhcx@mail.sdu.edu.cn (C.Z.)

\* Correspondence: lijy@sdu.edu.cn (Y.L.); sdzhaojl@sdu.edu.cn (J.Z.)

**Abstract:** Due to the inconsistency and intermittence of solar energy, concentrated solar power (CSP) cannot stably transmit energy to the grid. Heat storage can maximize the availability of CSP plants. Especially, thermochemical heat storage (TCHS) based on CaO/CaCO<sub>3</sub> cycles has broad application prospects due to many advantages, such as high heat storage density, high exothermic temperature, low energy loss, low material price, and good coupling with CSP plants. This paper provided a comprehensive outlook on the integrated system of CaO/CaCO<sub>3</sub> heat storage, advanced reactor design, heat storage conditions, as well as the performance of CaO-based materials. The challenges and opportunities faced by current research were discussed, and suggestions for future research and development directions of CaO/CaCO<sub>3</sub> heat storage were briefly put forward.

**Keywords:** thermochemical heat storage; CaO/CaCO<sub>3</sub> cycles; solar energy; CaO-based material



**Citation:** Yang, Y.; Li, Y.; Yan, X.; Zhao, J.; Zhang, C. Development of Thermochemical Heat Storage Based on CaO/CaCO<sub>3</sub> Cycles: A Review. *Energies* **2021**, *14*, 6847. <https://doi.org/10.3390/en14206847>

Academic Editor: David Chiaramonti

Received: 20 August 2021

Accepted: 6 October 2021

Published: 19 October 2021

**Publisher's Note:** MDPI stays neutral with regard to jurisdictional claims in published maps and institutional affiliations.



**Copyright:** © 2021 by the authors. Licensee MDPI, Basel, Switzerland. This article is an open access article distributed under the terms and conditions of the Creative Commons Attribution (CC BY) license (<https://creativecommons.org/licenses/by/4.0/>).

## 1. Introduction

In recent years, to deal with global warming and an increasing energy demand, the utilization of renewable resources, such as solar, hydrogen, biofuel, wind energy, and tidal energy, has made strides around the world [1]. Indeed, all countries have reached an agreement to control the temperature rise to 1.5 °C or below [2]. In addition, it has been reported that renewable energy power generation will account for 30% of the total global power generation, surpassing coal-fired power generation for the first time, by 2040 [3]. Nowadays, solar energy is extensively considered to be one of the most promising renewable resources due to its inexhaustibility, safety, and non-pollution. In particular, concentrated solar power (CSP) plants not only have the potential to be integrated into the grid for dispatching power generation [4,5], but have also seen a significant increase in deployment worldwide in recent years [6,7]. However, power production is unstable in the CSP plants due to the intermittent and inconsistent solar energy, which cannot reliably transmit energy to the grid [8,9]. Owing to this, heat storage has become worthy of attention and research that is obligatory, affordable, and efficient [10]. Thermal energy storage (TES) can store heat under sunshine during the day and release heat when there is no solar irradiation. To make solar energy available, it is generally believed that the integration of CSP and TES is a promising and effective option to overcome its limitations [11,12].

There are three forms of TES systems based on different heat storage principles: sensible heat storage (SHS), latent heat storage (LHS), and thermochemical heat storage (TCHS) [13]. SHS takes advantage of the temperature change of the heat storage material to store heat, which is the most mature for industrial applications. The heat storage capacity of SHS depends on the physical properties of the material itself. In addition, SHS materials commonly used in the CSP field mainly include heat transfer oil, molten salts, ceramic, and concrete [14]. LHS is a technology that uses the phase-change process of heat storage materials to store and release heat, so it is also called phase-change heat storage. LHS possesses constant charge/discharge temperature and large heat storage density. Phase

change materials (PCMs) mainly include organic, inorganic, and eutectic based on the chemical nature of the materials [15]. However, the traditional PCMs have some problems, such as low thermal conductivity and high energy loss [16]. Thus, the further industrial operation of CSP plants using LHS has been hindered.

In order to improve heat storage efficiency, it is necessary to research and develop new heat storage media with a higher heat storage temperature other than SHS and LHS. Moreover, TCHS absorbs heat through the decomposition of various chemical materials, which store heat energy in the form of chemical energy, and vice versa [17]. TCHS not only achieves a high heat storage density as well as small heat storage volume [12], but can also store energy for a long time at around room temperature [18]. Among the three systems as mentioned above, the special feature of TCHS is that it can store and transmit energy without loss of energy [19]. Therefore, TCHS is considered one of the most promising CSP heat storage technologies [20]. The main characteristics of the abovementioned three heat storage methods are summarized in Table 1 [21].

**Table 1.** The main characteristics of the three heat storage methods [19–21].

|                      | SHS   | LHS  | TCHS  |
|----------------------|---|--|---|
| Heat storage density | Low ~0.2 GJ/m <sup>3</sup>                          | Medium ~0.3–0.5 GJ/m <sup>3</sup>                                      | High ~0.5–3 GJ/m <sup>3</sup>   |
| Working temperature  | Low   | Low or medium  | Medium or high  |
| Advantages           | Mature technology<br>Low price<br>Long service life | Small heat storage volume<br>Simple system                             | High heat storage density<br>Small thermal losses<br>Long-distance transportation |
| Disadvantages        | High thermal losses<br>Low heat storage density     | Poor thermal conductivity<br>Material corrosion<br>High thermal losses | Complex technology<br>High cost   |

The different materials used in TCHS systems have been proven feasible, including carbonates [22,23], hydroxides [24,25], metal hydrides [26], metal oxides [27], ammonia [28], methanol [29], and sulfides [30]. Although the current TCHS technology is still immature and remains at the conceptual level, it is becoming an active research field. The common heat storage materials for TCHS are summarized in Figure 1 [31].

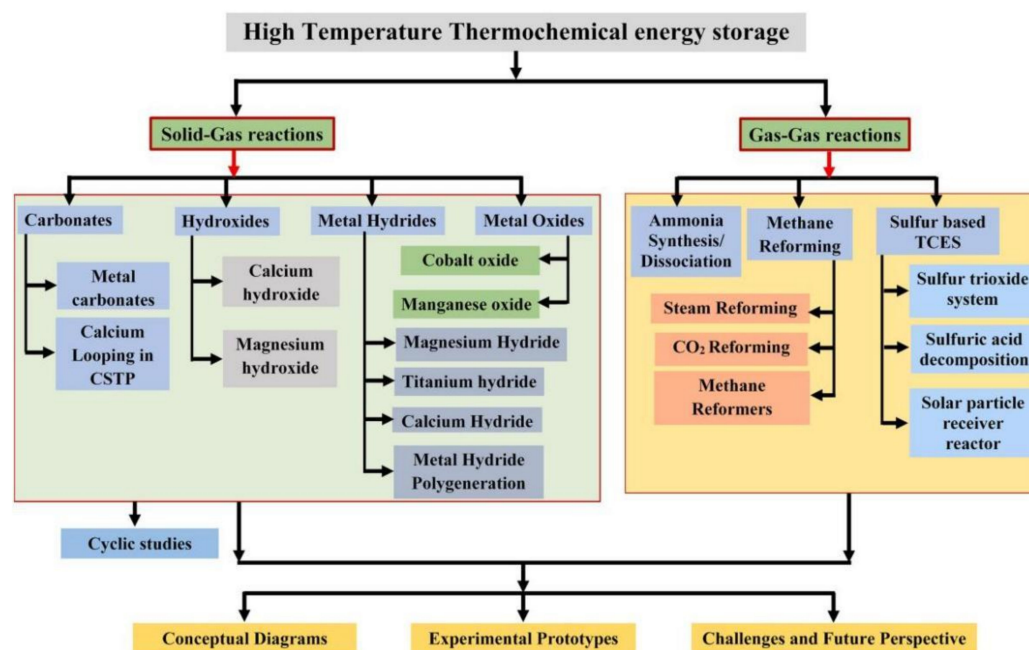


**Figure 1.** The common heat storage materials for TCHS [31].

Among various TCHS systems, high-temperature thermochemical heat storage based on the carbonation/calcination reaction of CaO/CaCO<sub>3</sub> (as exhibited in Equation (1)) is considered to be one of the promising CSP heat storage technologies [32]. CaO/CaCO<sub>3</sub> is one of the systems with the highest heat storage density (approximately 3.2 GJ/m<sup>3</sup>) [33] and the working temperature is relatively high [34], which is conducive to the realization of large-scale sustainable power generation. The equilibrium temperature of the reaction at atmospheric pressure under pure CO<sub>2</sub> is 895 °C [35]. The reaction equilibrium temperature is determined by the CO<sub>2</sub> partial pressure, as shown in Equation (2) [36].



$$P_{\text{eq}} = 4.137 \times 10^7 \exp\left(-\frac{20474}{T}\right) \quad (2)$$

where  $P_{\text{eq}}$  is the CO<sub>2</sub> partial pressure, bar;  $T$  is the equilibrium temperature, K. By changing the CO<sub>2</sub> partial pressure, the carbonator can proceed in the range of 600–900 °C [37]. Additionally, it takes advantage of abundant raw materials and low prices due to natural calcium-based minerals (limestone or dolomite) as the precursors, which can realize efficient heat storage [38].

Recently, many review articles related to TCHS have been published [39,40]. Among them, most of the reviews mainly studied the materials and prospects of a variety of TCHS systems [31,41], and a few focused on CaO/CaCO<sub>3</sub> heat storage systems. Hence, this paper reviews and summarizes the research progress of CaO/CaCO<sub>3</sub> heat storage in system integration, reaction conditions, and material properties, covering the most valuable aspects of such research.

## 2. CaO/CaCO<sub>3</sub> TCHS

System design represents a major contribution to the application of CaO/CaCO<sub>3</sub> heat storage in CSP plants. The concept of calcium looping (CaL) TCHS can be traced back to the 1970s [42], but most of the subsequent CaL research has focused on CO<sub>2</sub> capture [43]. Only with the increasing demand for heat storage in recent years has the application of CaL in TCHS been extensively studied. Although the CaO/CaCO<sub>3</sub> heat storage technology and the CO<sub>2</sub> capture technology have the same chemical reaction principle [44], they have remarkable differences in factors, such as reaction conditions and applications [45]. When the CaL process is utilized for CO<sub>2</sub> capture from the flue gas of coal-fired power plants, the carbonation stage of CaO occurs in a carbonator with the flue gas containing about 15 vol% CO<sub>2</sub> to form CaCO<sub>3</sub> at the optimal temperature of 600–700 °C [46,47]. The calcination stage of CaCO<sub>3</sub> occurs in a calciner at above 900 °C under a high concentration of CO<sub>2</sub> (>90 vol%) for CO<sub>2</sub> enrichment, where the required heat is provided by fuel oxygen-enriched combustion [48]. When CaL heat storage is implemented in CSP stations, its carbonation and calcination conditions are more flexible. The carbonation reaction is carried out under pure CO<sub>2</sub> for high temperature and power generation efficiency in the exothermic stage. Gases with different concentrations of CO<sub>2</sub> are fed into the carbonator as required, so the exothermic temperature of 600–900 °C can be reached [37]. Increasing the carbonation pressure can improve the limited temperature of the carbonation reaction [49].

In the solar calciner, the reactants generally cannot stay for a long time, so the calcination reaction in the CaO/CaCO<sub>3</sub> system needs to be accomplished as soon as possible [32]. Longer reaction time and higher temperature result in more severe sintering of CaO in the calcination stage, which is not beneficial for the carbonation of CaO [50]. Thus, a shorter time and lower temperature lead to a higher carbonation of CaO due to the slight sintering [51,52]. In addition, the solar calciner at low temperature needs fewer solar reflectors, so the cost is also reduced [53,54]. The calcination kinetics depends not only on the calcination temperature, but also on the calcination atmosphere [55]. The different calcination atmospheres for CaO/CaCO<sub>3</sub> heat storage were investigated, including CO<sub>2</sub> [55,56], steam [57], and inert gases [52]. For the calcination under pure CO<sub>2</sub> at atmospheric pres-

sure,  $\text{CaCO}_3$  can only be quickly decomposed at a temperature around  $930\text{--}950\text{ }^\circ\text{C}$  due to the limitation of thermodynamic equilibrium calculated by Equation (2) [52,55]. If the  $\text{CO}_2$  partial pressure is higher than the equilibrium pressure, the calcination reaction cannot occur. The utilization of superheated steam (SHS) can reduce the calcination temperature to as low as  $680\text{ }^\circ\text{C}$  to save energy, and the calcined  $\text{CaO}$  has strong heat storage activity [57]. Nevertheless, the separation of vapor and  $\text{CO}_2$  needs energy consumption. That is because the heat for cooling vapor is difficult to utilize.  $\text{CO}_2$  after separation and purification is easier to use and store [58]. The calcination temperature of  $\text{CaCO}_3$  can be noticeably reduced by using inert gases, such as helium (He) or nitrogen ( $\text{N}_2$ ). Compared with pure  $\text{N}_2$ , the calcination rate under pure He is faster due to the high diffusivity of  $\text{CO}_2$  in He and the high thermal conductivity of He, and the calcination temperature is as low as  $725\text{ }^\circ\text{C}$  [52]. However, a further issue that needs to be considered is the separation of  $\text{CO}_2$  and He. The content related to the reaction conditions will be discussed in detail in the next section. Recently, scholars have conducted lots of research on  $\text{CaO}/\text{CaCO}_3$  heat storage, continuously optimizing the integrated process of  $\text{CaO}/\text{CaCO}_3$  heat storage and CSP power generation to improve efficiency [59,60]. Furthermore, reducing the deactivation of  $\text{CaO}$  during heat storage and improving the heat storage stability have been widely studied.

### 2.1. CSP-CaL Schemes

The integration of CaL-CSP has attracted much attention due to the unique advantages of the  $\text{CaO}/\text{CaCO}_3$  heat storage system. The system coupling  $\text{CaO}/\text{CaCO}_3$  heat storage and CSP integrated power generation is developing rapidly, and its basic process is exhibited in Figure 2 [61]. The sunlight is converged on the solar calciner where  $\text{CaCO}_3$  decomposes into  $\text{CaO}$  and  $\text{CO}_2$  at a high temperature ( $\sim 725\text{--}950\text{ }^\circ\text{C}$  [52,61]). The generated  $\text{CaO}$  is stored at atmospheric pressure, and the released  $\text{CO}_2$  is stored after the compression. According to the needs of power generation,  $\text{CaO}$  and  $\text{CO}_2$  are fed into the carbonator ( $\sim 850\text{ }^\circ\text{C}$  or higher [52]). The heat released during the carbonation means the excess  $\text{CO}_2$  is heated to a high temperature, and then  $\text{CO}_2$  enters a turbine to achieve power output. Adding heat exchange systems after the heat storage and heat release process can improve the heat utilization rate.

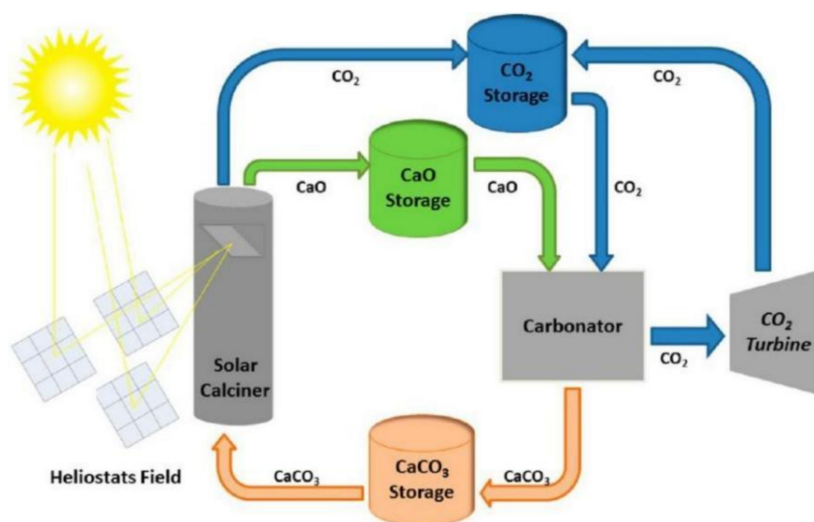


**Figure 2.** The integrated system of  $\text{CaO}/\text{CaCO}_3$  heat storage and CSP [61].

Edwards et al. [62] proposed an open  $\text{CO}_2$ /air Brayton cycle  $\text{CaO}/\text{CaCO}_3$  heat storage system, including a pressurized fluidized bed carbonator and a solar calciner, as shown in Figure 3. In the carbonation stage, the compressed  $\text{CO}_2$  and high-pressure air entered the reactor together. It assumed that  $\text{CO}_2$  was completely consumed in the carbonator, and then only high-temperature and high-pressure air was sent to the turbine to do work. Finally, the air experienced the Brayton cycle was discharged into the atmosphere.

The simulation results showed that when the material conversion rate was 20–40%, the carbonation temperature was 875 °C and the pressure was 6.7 bar. Moreover, the power generation efficiency of the system was maximum, up to 39.9–43.7%. It is worth noting that the complete consumption of CO<sub>2</sub> in the carbonator is an ideal situation. In fact, due to the thermodynamic balance of the reaction, CO<sub>2</sub> cannot completely react with CaO, so eventually the exhaust gas contains a large amount of CO<sub>2</sub>.

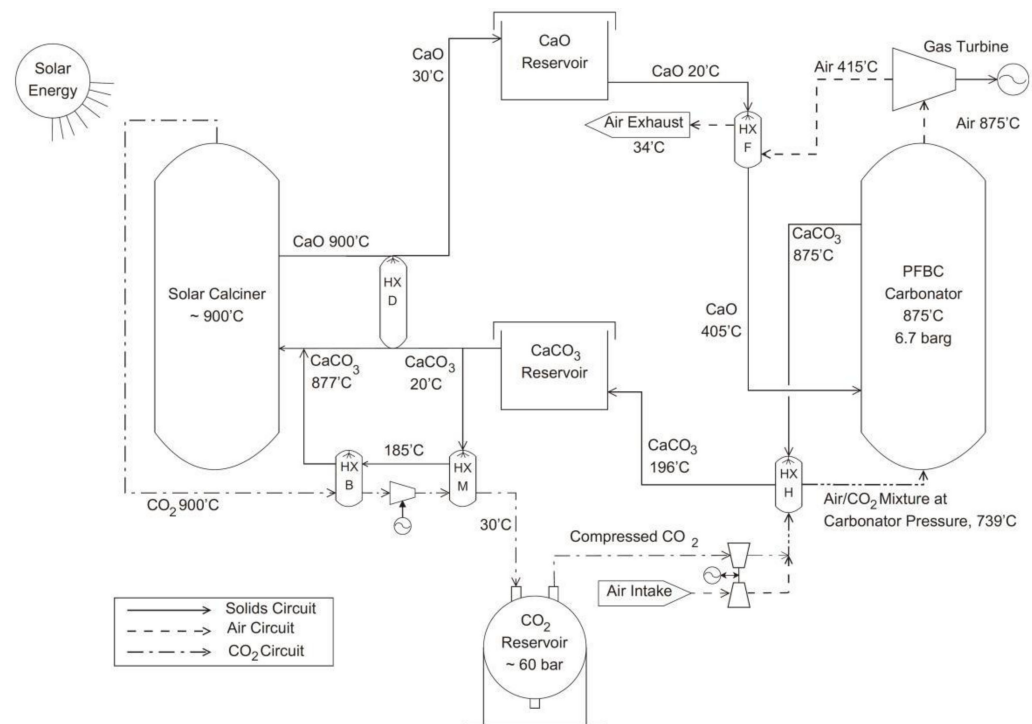


Figure 3. An open CO<sub>2</sub>/air Brayton cycle CSP-CaL system [62].

Chacartegui et al. [63] explored the CO<sub>2</sub> closed-loop Brayton cycle CSP-CaL system, as demonstrated in Figure 4. The excess CO<sub>2</sub> was sent to the carbonator, and the unreacted CO<sub>2</sub> was used as a heat carrier fluid to enter the CO<sub>2</sub> turbine for power generation. The exhausting CO<sub>2</sub> was compressed and stored to start the next cycle. It was also identified that calcium-based materials with high activity, high carbonation temperature, and high inlet pressure of CO<sub>2</sub> turbine were the substantial factors to guarantee high efficiency of the closed heat storage system. The calculation classified that the system efficiency could reach 46% when the ratio of CO<sub>2</sub> pressure to turbine outlet pressure was 3.2. Alovisio et al. [64] utilized the pinch-analysis methodology to optimize the heat transfer design in detail based on the closed CO<sub>2</sub> Brayton system, and the overall efficiency increased by 5% on the original basis.

Karasavvas et al. [65] integrated the Rankine cycle with the CO<sub>2</sub> Brayton cycle heat storage system and designed a scheme of continuous power generation with an efficiency of 31.5%. Tesio et al. [66] optimized the indirect integration of the steam Rankine cycle in CaL-CSP from both energy and economic aspects, which determined the size and operating conditions of the main components. Ortiz et al. [67] conducted an energy and sensitivity analysis on the closed system, and the results showed that various methods could be used to improve the system efficiency by adding gas-solid heat exchangers at both ends of the calciner and carbonator, increasing the turbine inlet temperature, and raising CaO conversion. Karasavvas et al. [68] also studied an exergy analysis on the system and found that most of the exergy loss occurred in the solar receiver (about 36.6%), the calcination section (i.e., 25.8%), and the steam Rankine cycle (about 20.6%). On the contrary, the exergy loss that occurred in the carbonation section was relatively small, about 4.8%. Cannone et al. [69] also used the pinch analysis method to study the integrated system and found that



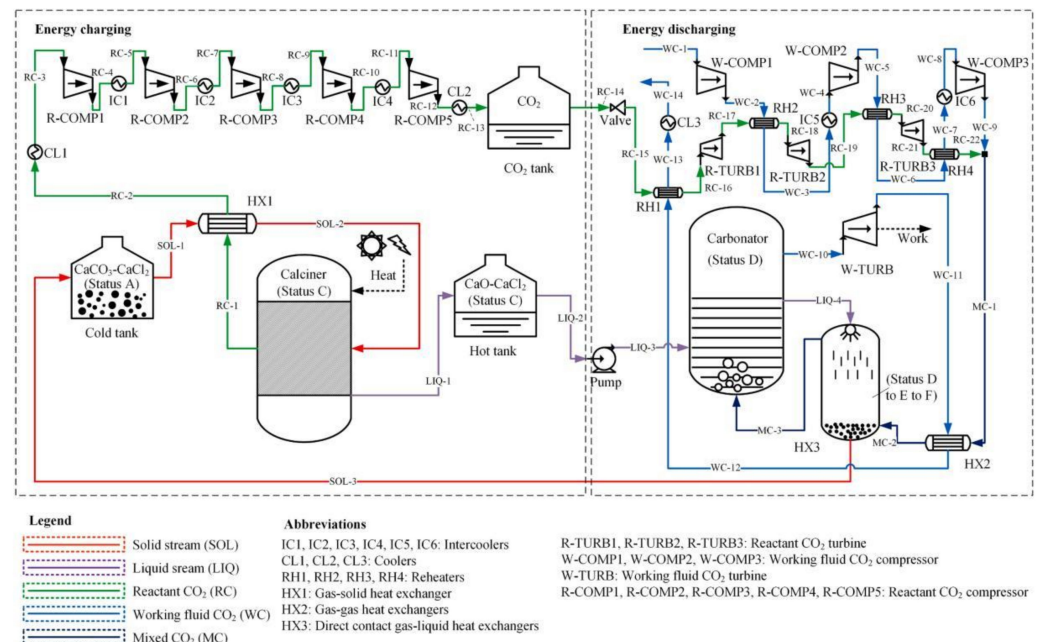
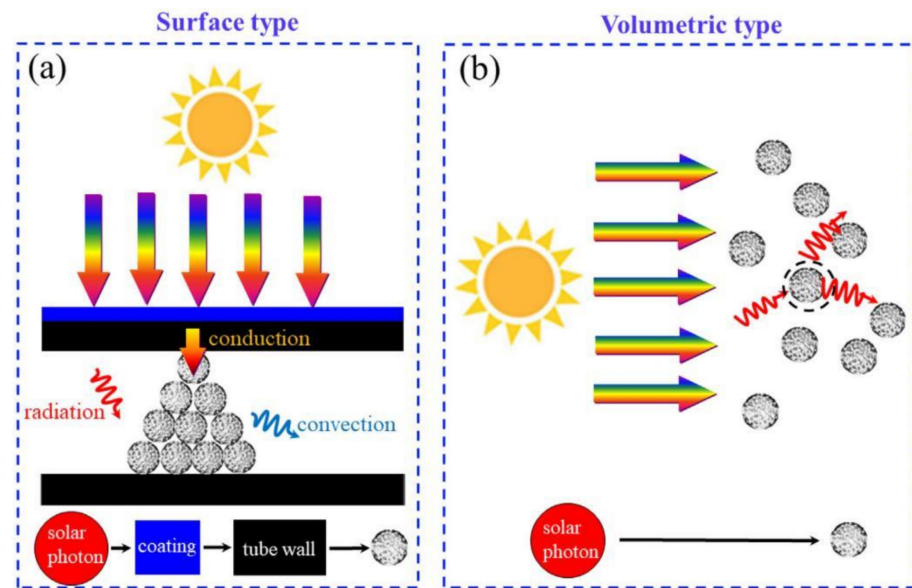


Figure 5. A phase change CSP-CaL system based on  $\text{CaO}/\text{CaCO}_3\text{-CaCl}_2$  [70].

## 2.2. CSP-CaL Equipment

The main equipment of the CSP-CaL system includes reactors, heat exchangers, storage systems, and conveying systems, which have been extensively studied in other industrial applications such as the cement industry [58]. The reactor of the CSP-CaL system is mainly used for the solid-gas reaction process, including the solar calciner and the carbonator. Among them, the carbonator has the same basic requirements as the existing CaL- $\text{CO}_2$  capture reactor, which is relatively mature technology [77]. The technology of solar calciner is still immature, although the calciner has been studied since the 1980s [78]. In addition, the solar calciner is the most critical equipment in the CSP-CaL system, and its overall design, especially the heat collection capacity, is sensitive to the efficiency of the system. According to the heat collection method, it can be divided into the surface type and volumetric type whose principles are shown in Figure 6 [79]. Figure 6a exhibits the surface type heat collection, where the sunlight is first absorbed by the surface coating of the reactor, and then the heat is transferred to the tube wall through heat conduction. Finally, the heat of the tube wall is transferred to the reactants in the form of thermal radiation and convection [80]. Figure 6b demonstrates the volumetric heat collection, in which the solar energy is directly radiated to the reactant, thereby eliminating the process for a large amount of heat transfer in the middle, but the ability of the reactant to receive solar radiation is higher [81]. For the surface heat collection, the high-temperature surface coating radiates a large amount of heat to the outside, causing serious heat loss [76]. The thermal resistance between the surface coating and the reactant is large, and the reactant may stick to the tube wall on account of sintering [82]. Thus, it is not suitable for the high-temperature  $\text{CaO}/\text{CaCO}_3$  heat storage system. The volumetric heat collection in which the reactant directly receives radiant energy is more suitable for this system.



**Figure 6.** Two heat collection methods of solar calciner [79]: (a) surface type; (b) volumetric type.

Ortiz et al. [32] described in detail the principles that should be followed in the design of the calciner, such as solid residence time, particle size, temperature gradient and so on. Lisbona et al. [83] designed a multi-stage solar calciner that could limit the peak temperatures for the reactors, alleviate the sintering of materials, and achieve the highest heat storage efficiency. In addition, due to the low solar optical absorption capacity of  $\text{CaCO}_3$ , it should also be considered in the design of the calciner [78].

The tiny solid particles are used in the solar calciner (particle receiver) to directly absorb the solar energy reflected by the heliostat, so as to rise to a very high temperature ( $\sim 900\text{ }^\circ\text{C}$  [62]). The heat can be stored in the tank or exchanged with the working medium. The temperature distribution in the receiver is related to the particle size and reaction time. Currently, there are many researches on the direct system of particle receivers as shown in Figure 7, mainly including falling particle receivers, fluidized bed receivers, rotary kiln receivers, etc.

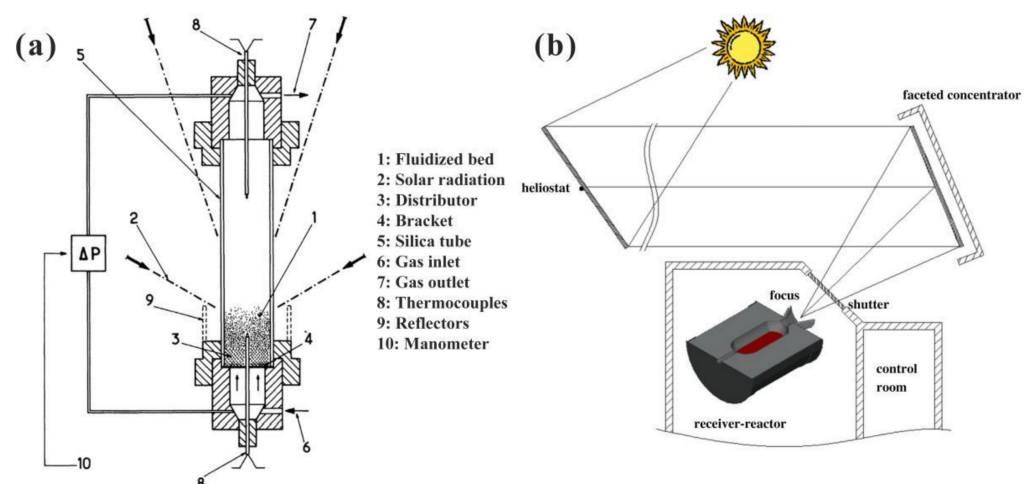


**Figure 7.** Solar calciner: (a) fluidized bed [78]; (b) rotary kiln [84].

The falling particle receiver is the most basic type of particle receiver, which receives solar radiation by letting solid particles fall directly. The thermal efficiency and outlet temperature of the working medium have a decisive relationship with the mass flow of particles and the residence time in the heated region [85]. In addition, in order to increase the outlet temperature of the working medium, one way is to increase the residence time

of particles, e.g., by setting the particles in the receiver to circulate multiple times [86]. Compared with the falling particle receiver, the solid particles in the fluidized bed receiver are blown by gas and in a suspended state, which is irradiated by concentrated sunlight. At this time, the solid particles are in full contact with the gas, which can effectively promote heat and mass transfer. Tregambi et al. [87] designed and used the  $\text{CaCO}_3$  carbonation/calcination reaction in a fluidized bed reactor with direct radiation to maximize solar energy collection. The study found that  $\text{CaO}/\text{CaCO}_3$  TCHS could be applied to fluidized bed receivers, whose heat storage density reached  $1000 \text{ J}/\text{m}^3$  in a quarter of the 12 cycles. However, due to uneven radiation, the bed layer was locally overheated, which aggravated the sintering of particles.

The principle of the rotary kiln receiver is to feed particles into the rotary kiln, and a light transmission window is set at one end of the receiver to concentrate sunlight. The centrifugal force of the rotary kiln receiver makes the particles rotate and fall along the wall of the receiver, and then the sunlight is injected through the light transmission window to heat the particles attached to the wall. At present, the rotary kiln has been widely used in the chemical and cement industry and is mostly used for calcination and decomposition reactions [88]. Therefore, it can be used as a solar calciner in a  $\text{CaO}/\text{CaCO}_3$  TCHS system. Moumin et al. [89] designed a high-temperature solar rotary kiln that was used for limestone calcination. An insulating layer was arranged between the reactor and the shell, and a quartz glass window was arranged to receive solar radiation. The experimental results showed that the total efficiency of the rotary kiln was 19–40%. The advantages and disadvantages of the different solar calciners are summarized in Table 2.

**Table 2.** Comparison in different solar calciners.

|                  | Advantages   | Disadvantages  |
|------------------|--|--|
| Falling particle | Simple structure design<br>Low energy consumption  | Poor heat transfer<br>Uneven solar radiation distribution  |
| Fluidized bed    | High heat and mass transfer efficiency<br>Mature industrial technology                               | Difficulty in gas-solid separation at high temperature<br>Serious particle wear<br>High requirements for flow rate control |
| Rotary kiln      | Low particle wear<br>Great heat and mass transfer<br>Suitable for materials with large particle size | Difficult to integrate design with the solar system<br>High equipment maintenance cost under high temperature              |

Furthermore, the description, schemes, and related issues of the reactor have been elaborated in detail in the literature [90]. Remarkably, the current research on solar calciner is still in its infancy. The structural design, light transmission window, and control system still need further research [91].

### 2.3. CSP-CaL Techno-Economics

At present, the research on the pilot-scale of CSP-CaL is still in its infancy [65,76], so only a rough discussion will cover its techno-economic analysis. When the CaL process is utilized for  $\text{CO}_2$  capture from the flue gas of coal-fired power plants, the research on techno-economic analysis is relatively extensive, which can be used as the reference for CSP-CaL. Hanak et al. [92] assessed the economic cost of retrofitting a 580 MW coal-fired power plant through CaL technology, which may be between 2100–2300 €/kW. Michalski et al. [93] thoroughly evaluated the economic investment of a power plant based on CaL technology by using the break-even electricity price method, and its capital cost was 2573.5 €/kW. Bayon et al. [94] conducted a techno-economic assessment of 17 solid-gas TCES systems. It was found that the cost of raw materials and the energy consumption of auxiliary equipment had the greatest impact on the capital cost of the system. The CaL process was determined to be competitive with molten salt at the lowest cost. Unfortunately, the energy consumption of auxiliary equipment based on carbonate systems was very high, especially

the high energy required to compress CO<sub>2</sub>. Tesio et al. [95] conducted an economic analysis on the CaL indirect integrated CSP plant, including the supercritical CO<sub>2</sub> Brayton cycle and steam Rankine cycle. It was found that the calciner and the solar energy sides accounted for 86% of the total investment capital. In addition, not only was the investment cost of each component estimated, but also the economic optimization of the calcination reaction device, including the optimal size of the calciner and compressor components. The results of the economic analysis showed that the supercritical CO<sub>2</sub> Brayton cycle was the optimal choice for indirect integration. Muto et al. [96] studied the heat exchange reactor for waste heat recovery and the reactant transportation method, then optimized and economically analyzed the CaO/CaCO<sub>3</sub> heat storage system. It is estimated that the expected investment cost per kW·h of heat energy stored in a commercial-scale system, including equipment and installation, emergency, heat storage materials, land, and other expenses, is about 47 \$/(kW·h).

In the techno-economic analysis of CSP-CaL, the CaL process has advantages due to the low cost of materials (calcium-based precursors such as limestone). The disadvantage of the CaL process is the high energy consumption of auxiliary equipment (including CO<sub>2</sub> compression). Therefore, more effective integration of the CSP-CaL scheme is needed, including storage systems, solids transportation, and gas separation.

### 3. Effect of Reaction Conditions on Performance of CaO-Based Materials in CaO/CaCO<sub>3</sub> TCHS

For the CaO/CaCO<sub>3</sub> TCHS system, whether the CaO-based material can maintain high carbonation performance and cyclic stability are key to heat storage. A number of studies have shown that temperature [97], pressure [98,99], atmosphere [100], and particle size [101] have crucial effects on the sintering rate of CaO-based materials. Therefore, it is necessary to study the reaction conditions in the stages of calcination and carbonation.

The heat storage performances of CaO-based materials are evaluated by the effective conversion [97] and heat storage density [98], respectively. The effective conversion denotes the ratio of the mass of CaO reacted during each carbonation cycle to the total mass of the sample before the carbonation, which is defined by Equation (3):

$$X_{\text{ef},N} = \frac{m_{\text{car},N} - m_{\text{cal},N-1}}{m_0} \cdot \frac{M_{\text{CaO}}}{M_{\text{CO}_2}} \quad (3)$$

where  $N$  denotes the number of TCHS cycles;  $X_{\text{ef},N}$  is the effective conversion of CaO-based materials after  $N$  TCHS cycles;  $m_{\text{car},N}$  and  $m_{\text{cal},N-1}$  denote the mass of the sample after the  $N$ th carbonation and the  $N-1$ th calcination, respectively, g;  $m_0$  represents the original mass of the sample, g;  $M_{\text{CaO}}$  and  $M_{\text{CO}_2}$  represent the molar masses of CaO and CO<sub>2</sub>, respectively, g/mol.

Heat storage density represents the maximum heat that can be released per unit mass of CaO-based materials during each carbonation reaction, which is defined by Equation (4):

$$E_{\text{g},N} = X_{\text{ef},N} \cdot \frac{1000\Delta H^0}{M_{\text{CaO}}} \quad (4)$$

where  $E_{\text{g},N}$  is the heat storage density of CaO-based materials, kJ/kg;  $\Delta H^0$  denotes the standard reaction heat (178 kJ/mol for 0 °C; 165.5 kJ/mol for 900 °C).

#### 3.1. Effect of Calcination Conditions

Calcination conditions, including harsh and mild calcination conditions, usually play an important role in the heat storage properties of CaO-based materials. Valverde et al. [61] found that the thermal pretreatment of limestone could improve heat storage performance. The effective conversion of limestone thermally pretreated for 1 h under N<sub>2</sub> at 760 °C was 0.58 after 20 cycles, which was 90% higher than that of limestone without thermal pretreatment. Sarrión et al. [102] studied the influence of calcination conditions

on the heat storage performance of the limestone and the Ca/Al composites. It was found that the effective conversion of the limestone calcined under pure He at 725 °C decreased from 0.70 to 0.21 after 20 cycles. However, when the limestone was calcined under pure CO<sub>2</sub> at 950 °C, its effective conversion dropped from 0.69 to 0.18 after 20 cycles. This was because the calcination at high temperatures under high concentrations of CO<sub>2</sub> aggravated the sintering of CaO, which was more obvious in the study of limestone Ca/Al composites. When the Ca/Al composites were calcined under pure CO<sub>2</sub> at 950 °C, the effective conversion decreased from 0.60 to 0.18 after 20 cycles. However, under pure He at 725 °C, its effective conversion dropped from 0.74 to 0.41 after 20 cycles. This may be because the Tammann temperature (~771 °C) of Ca<sub>3</sub>Al<sub>2</sub>O<sub>6</sub> was lower than the calcination temperature used in the test (950 °C). When the reaction temperature of solid particles reaches a certain temperature, each atom in the crystal lattice begins to show a significant diffusion effect, and the chemical reaction properties become stronger, which is the Tammann temperature [103]. The Tammann temperature is a crucial factor affecting sintering. Valverde et al. [104] demonstrated the effect of SHS in the calcination atmosphere on the heat storage performance of limestone. When 0.03 vol% steam was added into the three calcination atmospheres, i.e., N<sub>2</sub>, He, and CO<sub>2</sub>, respectively, the calcination rates of limestone were all obviously accelerated. The limestone was completely calcined at 700 °C under wet N<sub>2</sub>, while under wet He, the calcination temperature could be reduced to 680 °C. The calcination rate of limestone under wet CO<sub>2</sub> was nearly three times higher than that under dry CO<sub>2</sub>, and the calcination temperature could be reduced to 925 °C. Sarrion et al. [105] proposed a new method to calcine limestone under CO<sub>2</sub> at low pressure. When the CO<sub>2</sub> pressure was 0.01 bar, the decomposition of limestone occurred at 765 °C, and the thermal storage stability of limestone was also noticeably improved. However, it should be noted that to maintain the low pressure of the calciner, more energy consumption would be needed. It is difficult to ensure the flowability of the heat storage material under negative pressure, which may be hardly possible to realize large-scale industrial applications. Champagne et al. [106] pointed out that the presence of high concentration of steam remarkably promoted the cyclic heat storage stability during the calcination stage in a thermogravimetric analyzer (TGA). However, the structure of the generated CaO was changed negatively, suggesting a decrease in the mechanical strength of CaO. It may cause severe particle fragmentation, so the smaller particles easily escape from the reactor, which is not conducive to its application in the fluidized bed reactor [107]. He et al. [47] used density functional theory to study the catalytic effect of steam on the decomposition of CaCO<sub>3</sub> and its mechanism at the molecular level. Obermeier et al. [108] found that the hydration treatment of calcium-based materials during energy storage could reactivate low-activity CaO. After five heat storage cycles, CaO was hydrated in steam at 250 °C, and the heat storage performance of limestone was improved by 39%.

### 3.2. Effect of Carbonation Conditions

At present, the carbonation of CaO/CaCO<sub>3</sub> heat storage research is mostly carried out under atmospheric pressure. Compared with carbonation at atmospheric pressure, CaO/CaCO<sub>3</sub> TCHS benefits from carbonation at increased pressure. Sarrion et al. [109] studied the heat storage performance of limestone and dolomite at the carbonation pressure of 3 bar (calcination under CO<sub>2</sub> at 1000 °C, carbonation under CO<sub>2</sub> at 850 °C). The effective conversion of calcium-based material was lower than that under 1 bar carbonation as the increase of pressure intensified the sintering of CaO. In addition, Sun et al. [98] performed heat storage experiments with limestone in a pressurized fixed bed and found that increasing the carbonation pressure could make carbonation occur at a temperature of 950 °C or higher. At the same time, increasing the carbonation pressure from 0.1 to 1.3 MPa, the heat storage capacity of limestone was also drastically enhanced, as exhibited in Figure 8. After 30 cycles, the effective conversion and energy density of limestone under 1.3 MPa were 0.61 and 1939 kJ/kg, respectively, which were 1.44 times as high as those under 0.1 MPa.

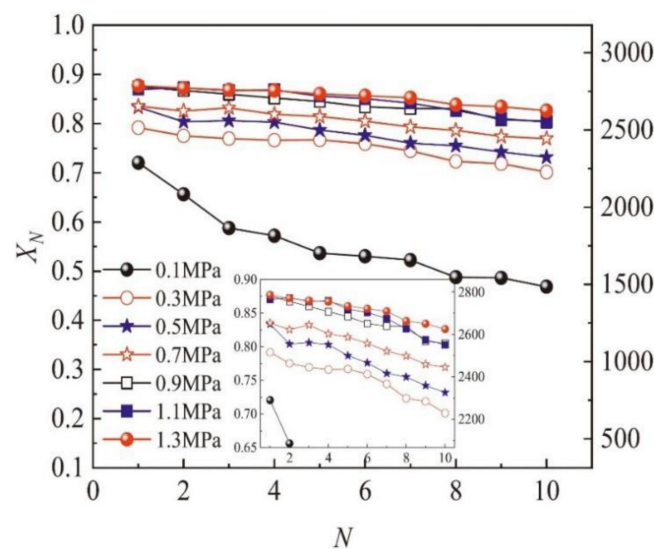


**Figure 8.** Influence of carbonation pressure on cyclic heat storage performance of limestone (calcination under pure N<sub>2</sub> at 850 °C for 10 min, carbonation under pure CO<sub>2</sub> at 850 °C for 5 min) [98].

Li et al. [110] studied the heat storage properties of CaO pellets under pressurized carbonation (1.3 MPa) and harsh calcination conditions (950 °C, pure CO<sub>2</sub>). They found that the energy density of CaO pellets carbonated after 10 cycles was 1423 kJ/kg, which was lower than that of limestone powder, but the compressive strength and wear resistance of CaO pellets during the cycles were higher. Furthermore, increasing the pressure and temperature of carbonation was more suitable for practical industrial application conditions. Pressurized carbonation as the reaction condition is used in process simulation [62]. Therefore, the heat storage performance of calcium-based materials under high carbonation pressure is worthy of attention and research.

### 3.3. Effect of Particle Size

Benitez-Guerrero et al. [97] studied the heat storage performances of two kinds of limestone with different particle sizes (<45 μm and >45 μm) and found that the effective conversion of limestone particles (>45 μm) decreased significantly, and its effective conversion dropped from 0.76 to 0.16 in 20 heat storage cycles. However, the effective conversion of the limestone particles (<45 μm) decreased from 0.8 to 0.42, which showed that the particle size of limestone had a significant impact on heat storage. This was because the larger CaO particles were rapidly deactivated due to pore plugging, which limited the carbonation/calcination of the heat storage process. Durán-Martín et al. [111] examined the effect of particle size on the heat storage performance of limestone calcined in pure helium and found that limestone with a smaller particle size (<15 μm) had a higher multicyclic activity in the heat storage cycles. Ma et al. [107] studied the heat storage performance of limestone under bubbling fluidization. They found that with increasing the fluidization velocity from 0.04 to 0.06 m/s, the heat storage capacity of limestone increased by 12%, but the attrition rate was accordingly improved by 96%. When the CO<sub>2</sub> concentration increased from 80% to 100%, the heat storage performance of limestone rose by 11%. Compared with the limestone with a particle size of 0.18–0.25 mm, the limestone with the relatively smaller particle size of 0.125–0.18 mm exhibited slightly higher heat storage capacity. This was because the relatively smaller limestone particles in the fluidization state showed better mass and heat transfer performances, resulting in higher CaO reactivity for heat storage.

## 4. Performance of CaO-Based Materials in CaO/CaCO<sub>3</sub> TCHS

It has been a consensus that the effective conversion of CaO plays a decisive role in the CaO/CaCO<sub>3</sub> cycles heat storage. Prieto et al. [112] pointed out that the inactivation of CaO was a major defect for the CSP-CaL system. As the number of CaO/CaCO<sub>3</sub> heat

storage cycles increases, the activity of CaO decreases rapidly, and usually reaches a lower conversion over 20 cycles [113]. On the one hand, the carbonation occurs rapidly under high CO<sub>2</sub> pressure at high temperature, so the generated CaCO<sub>3</sub> layer blocks pores of the unreacted CaO [61]. On the other hand, due to the low Tammann temperature of calcium-based materials, CaO grains are sintered under harsh calcination conditions during multiple CaO/CaCO<sub>3</sub> heat storage cycles [50]. The deactivation characteristics of CaO in the heat storage cycles are mainly related to the CaO precursor and the calcination/carbonation conditions. Calcium-based materials include a variety of natural ores, such as limestone, dolomite, and calcium-rich industrial waste such as carbide slag, steel slag, and fly ash [114].

#### 4.1. Natural CaO-Based Materials

Benitez-Guerrero et al. [97] compared the cyclic heat storage performance of natural calcium-based materials, such as limestone and dolomite. After the 20 heat storage cycles, the effective conversion of limestone (<45 μm) dropped from 0.8 to 0.42. The cyclic effective conversion of dolomite was more stable, which decreased by 28% after 20 cycles. This was because that the MgO in dolomite could relieve the sintering and pore plugging of CaO. However, the initial effective conversion of dolomite was not high, about 0.6.

In addition, Benitez-Guerrero et al. [115] also compared the cyclic heat storage performance of natural calcium carbonate minerals such as limestone, chalk, and marble, and their thermograms were shown in Figure 9. The initial reaction kinetics and conversion rates of the three calcium-based materials were very similar, as presented in Figure 9a. The carbonation reaction of CaO derived from calcium carbonate minerals was almost completely carried out in the chemical reaction-controlled stage, while that in the diffusion-controlled stage could be ignored. This provided a crucial reference for the optimization of reactor design. However, as demonstrated in Figure 9b, the inactivation degree of the CaO derived from three calcium carbonate minerals was significantly different in their crystallinities and sizes of the CaO grains. Limestone had the higher effective conversion (0.51) while marble had the lowest conversion (0.27). Durán-Martín et al. [111] tested the heat storage performance of limestone particles with different particle size distributions in multiple cycles and studied the effect of particle size on the deactivation mechanism of limestone. It was found that when calcined under He at low temperature, the utilization of small particles of limestone was more beneficial for heat storage, but this promotion was only effective for limestone particles below 15 μm.

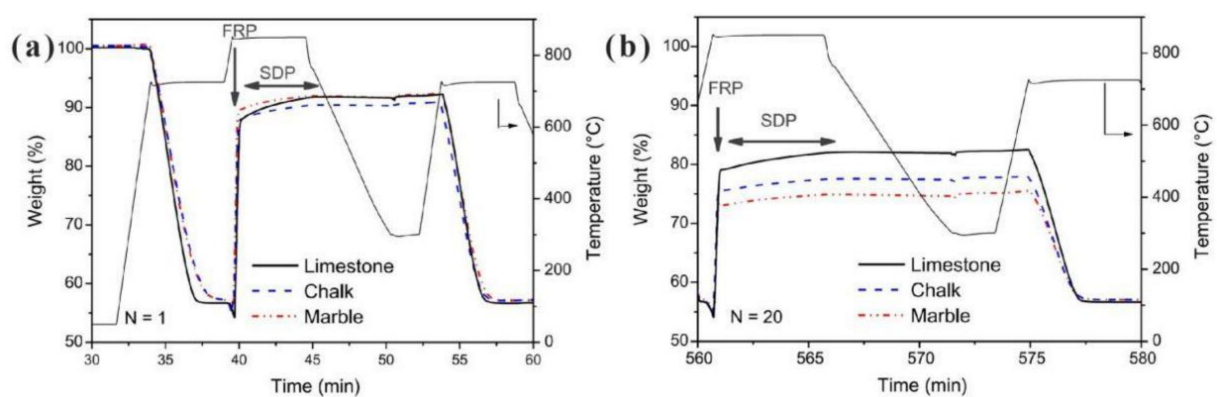


Figure 9. The temperature and weight of three samples vs. reaction time [115]: (a) the first cycle; (b) the last cycle.

#### 4.2. Waste CaO-Based Materials

Besides natural calcium-based materials, such as limestone and dolomite, another type of industrial waste with high calcium content can also be applied for heat storage through the CaL process [116]. Among them, steel slag is a common industrial waste, most of which is used to pave roads and produce concrete. Carbide slag is a waste produced by polyvinyl chloride and chlor-alkali whose main component is Ca(OH)<sub>2</sub>. A large amount

of carbide slag is directly piled-up or buried nearby, resulting in serious environmental damage and waste of resources. The application of calcium-based industrial waste residues for CaO/CaCO<sub>3</sub> heat storage not only saves calcium sources, but also realizes the resource utilization of waste residues. Perejon et al. [117] studied the cyclic heat storage performance of industrial waste steel slag. They found that the treated steel slag with acetic acid achieved an effective conversion rate of 0.8 after 20 heat storage cycles. Thus, the treated steel slag is an ideal heat storage material for CaL-CSP. Valverde et al. [118] compared the heat storage performances of blast furnace slag and calcium-rich steel slag. After acetic acid treatment, the heat storage performances of steel slag and blast furnace slag became more stable, but the maximum effective conversion rate was only about 0.30, which was lower than that of limestone. Although Al and Mg oxides in the waste slag improved its cyclic heat storage stability, the low contents of CaO in the waste slag limited the maximum heat storage capacity. In the abovementioned acetic acid treatment process, a filtration step was added to remove silicon impurities, which could increase the effective conversion of the waste residue after treatment to about 0.60. Bai et al. [119] also reported the influence of different acidification parameters, such as acid concentration, acidification temperature, and acidification time on the heat storage of calcium-based composites derived from steel slag. Among them, after the steel slag was acidified with acetic acid, the contents of Ca and Mg increased, while the contents of Si and Fe decreased, which improved its cyclic stability. Sun et al. [98] examined the cyclic heat storage performance of carbide slag and found that the presence of chlorine resulted in a rapid drop in the heat storage performance in the first two cycles, whereby it remained stable during 30 cycles. Consequently, carbide slag is a promising calcium-based heat storage material. Jahromy et al. [120] studied the heat storage potential of fly ash by using X-ray fluorescence (XRF) spectroscopy, scanning electron microscopy (SEM), and so on. Furthermore, they confirmed that the content of CaO in fly ash was 27%, indicating that it was promising as a heat storage material. However, more experimental studies were still required for the industrial application. Similarly, Maaten et al. [121] also explored the possibility of oil shale ash heat storage through the use of XRF, elemental analysis, and thermal analysis. Troya et al. [122] examined the heat storage properties of CaO derived from biomineralized CaCO<sub>3</sub>, such as snail shells and eggshells. They found that after 20 cycles, the conversion rate was equivalent to that of limestone, indicating that this type of food waste was feasible for heat storage. Utilizing CaO-based waste as heat storage material in CaO/CaCO<sub>3</sub> TCHS can not only save a lot of limestone resources, but also make full use of waste, which greatly solves the practical problem of waste accumulation. Table 3 summarizes the heat storage properties of several common natural and waste CaO-based materials reported in the literature.

**Table 3.** Comparison of heat storage properties of natural and waste CaO-based materials reported in the literatures.

| CaO-Based Materials | Particle Size | Calcination Conditions        | Carbonation Conditions        | Cycles | Effective Conversion | Reference |
|---------------------|---------------|-------------------------------|-------------------------------|--------|----------------------|-----------|
| Limestone           | <45 μm        | 725 °C/He/5 min               | 850 °C/CO <sub>2</sub> /5 min | 20     | 0.41                 | [97]      |
|                     | >45 μm        | 725 °C/He/5 min               | 850 °C/CO <sub>2</sub> /5 min | 20     | 0.18                 | [97]      |
|                     | >160 μm       | 725 °C/He/5 min               | 850 °C/CO <sub>2</sub> /5 min | 20     | 0.21                 | [102]     |
|                     | >160 μm       | 950 °C/CO <sub>2</sub> /5 min | 850 °C/CO <sub>2</sub> /5 min | 20     | 0.18                 | [102]     |
|                     | 100–400 μm    | 1000 °C/CO <sub>2</sub>       | 850 °C/CO <sub>2</sub> /1 bar | 11     | 0.13                 | [109]     |
|                     | 100–400 μm    | 1000 °C/CO <sub>2</sub>       | 850 °C/CO <sub>2</sub> /3 bar | 11     | 0.07                 | [109]     |
|                     | -             | 725 °C/He/5 min               | 850 °C/CO <sub>2</sub> /5 min | 20     | 0.51                 | [115]     |

Table 3. Cont.

| CaO-Based Materials | Particle Size         | Calcination Conditions        | Carbonation Conditions               | Cycles | Effective Conversion | Reference |
|---------------------|-----------------------|-------------------------------|--------------------------------------|--------|----------------------|-----------|
| Dolomite            | <45 $\mu\text{m}$     | 725 °C/He/5 min               | 850 °C/CO <sub>2</sub> /5 min        | 20     | 0.41                 | [97]      |
|                     | >45 $\mu\text{m}$     | 725 °C/He/5 min               | 850 °C/CO <sub>2</sub> /5 min        | 20     | 0.42                 | [97]      |
|                     | 100–400 $\mu\text{m}$ | 1000 °C/CO <sub>2</sub>       | 850 °C/CO <sub>2</sub> /1 bar        | 11     | 0.20                 | [109]     |
|                     | 100–400 $\mu\text{m}$ | 1000 °C/CO <sub>2</sub>       | 850 °C/CO <sub>2</sub> /3 bar        | 11     | 0.15                 | [109]     |
| Marble              | -                     | 725 °C/He/5 min               | 850 °C/CO <sub>2</sub> /5 min        | 20     | 0.27                 | [115]     |
| Chalk               | -                     | 725 °C/He/5 min               | 850 °C/CO <sub>2</sub> /5 min        | 20     | 0.38                 | [115]     |
| Steel Slag          | -                     | 675 °C/He/5 min               | 850 °C/CO <sub>2</sub> /5 min        | 20     | 0.63                 | [117]     |
| Steel Slag          | -                     | 650 °C/He/5 min               | 850 °C/CO <sub>2</sub> /5 min        | 20     | 0.50                 | [118]     |
| Blast Furnace Slag  | -                     | 650 °C/He/5 min               | 850 °C/CO <sub>2</sub> /5 min        | 20     | 0.29                 | [118]     |
| Carbide Slag        | <125 $\mu\text{m}$    | 850 °C/N <sub>2</sub> /10 min | 850 °C/CO <sub>2</sub> /5 min/13 bar | 30     | 0.51                 | [98]      |
| Snail Shell         | 20 $\mu\text{m}$      | 750 °C/N <sub>2</sub> /5 min  | 850 °C/CO <sub>2</sub> /5 min        | 20     | 0.24                 | [122]     |
| Eggshell            | 20 $\mu\text{m}$      | 750 °C/N <sub>2</sub> /5 min  | 850 °C/CO <sub>2</sub> /5 min        | 20     | 0.19                 | [122]     |

## 5. Improvement on Cyclic Thermal Storage Stability of CaO-Based Materials in CaO/CaCO<sub>3</sub> TCHS

The heat storage performance of natural calcium-based materials, such as limestone and dolomite, declines rapidly with the number of heat storage cycles, which has an adverse effect on the CaO/CaCO<sub>3</sub> TCHS. The lower the performance of CaO, the higher the inert solid content of the heat storage system for transportation, preheating, and cooling, resulting in a large amount of energy loss [67]. Studies have shown that the overall efficiency of CSP-CaL power plants increased by more than 10%, as the effective conversion of calcium-based materials increased from 0.07 to 0.5 [63]. Thus, it is beneficial to improve the cyclic heat storage performance of calcium-based materials and prepare calcium-based heat storage materials with high efficiency and stable performance, which have become the focus of attention of researchers. Adding a dopant with a high Tammann temperature to calcium-based materials is one of the most common methods to slow down the sintering of CaO-based materials. The supporter dispersed between the CaO grains plays a supporting role, which prevents the agglomeration of the CaO grains at high temperatures to a certain extent and enhances the sintering resistance of the CaO-based material [123].

### 5.1. CaO/SiO<sub>2</sub> Composites

SiO<sub>2</sub> is one of the reliable supporters with a wide range of sources and good application prospects. Studies have found that molecular sieves and nano-structured SiO<sub>2</sub> can be used to improve the structural dispersion of CaO particles and reduce sintering [124,125]. Benitez-Guerrero et al. [126] synthesized cheap porous CaO/SiO<sub>2</sub> composites using the biotemplate (rice husk) method. The heat storage performance of the composite material (70% content of CaO) was significantly better than that of limestone. After 20 cycles, the effective conversion of CaO was about 0.5. In addition, its heat storage density was about 40% higher than that of limestone after 50 cycles. This was because the composite material had a porous structure, in which the evenly dispersed SiO<sub>2</sub> alleviated the sintering and pore plugging of CaO. Chen et al. [127] doped SiO<sub>2</sub> into CaCO<sub>3</sub> by the mechanical mixing method and studied its kinetics, thermodynamics, and cycling stability in TGA. The composite material supplemented with 5 wt.% SiO<sub>2</sub> possessed the best heat storage performance. After the addition of 5 wt.% SiO<sub>2</sub>, the cyclic stability of CaCO<sub>3</sub> was enhanced by 28% and the attenuation rate reached 0.85% per cycle. However, the addition of SiO<sub>2</sub> led to a decrease in the calcination conversion rates of calcium-based materials. The heat release of the CaO/SiO<sub>2</sub> composite was still higher than that of CaO because the specific heat capacity of the composites increased by 20%. This may be because the thermal conductivity of SiO<sub>2</sub> (10.2 W/m·K) was higher than that of CaCO<sub>3</sub> (2.259 W/m·K [128]).

Khosa et al. [129] prepared the composite by wet mixing method with  $\text{CaCO}_3$  and nano- $\text{SiO}_2$  (the molar ratio of Ca to Si = 1:1). It was found that the heat storage capacity of the doped sample decreased by 43% after 20 cycles, while that of  $\text{CaCO}_3$  dropped by 56%. In addition, due to the high thermal conductivity of  $\text{SiO}_2$ , CaO could reach the reaction temperature faster. Therefore,  $\text{SiO}_2$  enabled the composite materials to be completely calcined at a lower calcination temperature. For instance, the decarbonation temperature of  $\text{CaCO}_3$  could be reduced from 750 °C to 700 °C due to  $\text{SiO}_2$  under Ar. Møller et al. [130] studied the influence of 11 different additives such as  $\text{SiO}_2$ ,  $\text{Fe}_2\text{O}_3$ ,  $\text{BaCO}_3$ ,  $\text{ZnO}$ , etc. on the heat storage performance of limestone. Among them, the most ideal additives were  $\text{Al}_2\text{O}_3$  (20 wt%) and  $\text{ZrO}_2$  (40 wt%), which could better resist the attenuation of  $\text{CaCO}_3$ , so that the capacity degradation rate after 500 cycles was only 20%.

### 5.2. CaO/ $\text{Al}_2\text{O}_3$ Composites

Obermeier et al. [109] examined CaO/ $\text{Al}_2\text{O}_3$  composites prepared from calcium acetate and aluminum nitrate and found that the heat storage density of the composite with the molar ratio of Ca/Al = 95:5 after 20 cycles was 3.5 times that of the unmodified CaO. Benitez-Guerrero et al. [131] utilized a mechanical mixing method to prepare CaO/ $\text{Al}_2\text{O}_3$  composite materials. It was found that  $\text{Ca}_4\text{Al}_6\text{O}_{13}$  was formed in the mild calcination stage of CaO and  $\text{Al}_2\text{O}_3$ , which could alleviate the high-temperature sintering of CaO and improve the heat storage stability of the composite. The effective conversion of the sample with the 5 wt%  $\text{Al}_2\text{O}_3$  was 0.55 after 20 cycles. Fedunik-Hofman et al. [132] used  $\text{Ca}(\text{NO}_3)_2$ ,  $\text{Al}(\text{NO}_3)_3$ , and  $(\text{NH}_4)_2\text{HPO}_4$  as precursors to prepare a Ca/Al/P composite by using the Pechini method. It was found that for the calcination under pure  $\text{CO}_2$  at 1000 °C, the composite still had an effective conversion of 0.67 after 20 heat storage cycles, while that of limestone was only 0.10. It was noted that the apatite was formed during the preparation process, and its melting point was 1650 °C, which effectively alleviated the high-temperature sintering of CaO. In addition, the apatite precursors were cheaper than calcium aluminate precursors, which could be used as a substitute for calcium aluminate to improve the thermal storage stability of calcium-based materials. Han et al. [133] compared the promotion effects of  $\text{Al}_2\text{O}_3$ ,  $\text{SiO}_2$ , and  $\text{TiO}_2$  on the heat storage performance of calcium-based materials, and found that, among the three additives,  $\text{Al}_2\text{O}_3$  had the best influence on enhancing the heat storage stability of the samples. After 50 cycles, the heat storage density of the composite with 5 mol% Al was 1500 kJ/kg, which was equivalent to 87% of the theoretical maximum. Sun et al. [134] studied composite heat storage materials prepared from limestone (as calcium precursor), calcium aluminate (as supporter), and  $\text{CeO}_2$  (as catalyst). They found that  $\text{CeO}_2$  could generate oxygen vacancies on the surface of calcium-based materials to promote the transfer of  $\text{O}^{2-}$ , which improved the heat storage performance of calcium-based materials. Under the synergistic effect of  $\text{CeO}_2$  and  $\text{Ca}_{12}\text{Al}_{14}\text{O}_{33}$ , the composite achieved the maximum heat storage capacity when the addition amount of both  $\text{Al}_2\text{O}_3$  and  $\text{CeO}_2$  was 5 wt%. After 30 heat storage cycles, the effective conversion and heat storage density of the composite were as high as 0.79 and 2500 kJ/kg, respectively. In addition, Sun et al. [135] further used absorbent paper as a template to prepare a Ca/Al/Ce composite heat storage material with a porous hollow tube structure. They found that the optimal addition amounts of  $\text{Al}_2\text{O}_3$  and  $\text{CeO}_2$  were 2.5 wt% and 1 wt%, respectively. The effective conversion and heat storage density of the Ca/Al/Ce composite with hollow tube after 30 cycles retained 0.92 and 2924 kJ/kg, respectively. Møller et al. [136] studied the energy storage performance and material physical properties of a calcium-based thermochemical energy storage system using a packed bed reactor under three operation scenarios, equipped with 3.2 kg of composite material (0.82 kWh thermal energy) by hand-mixing  $\text{CaCO}_3$  and  $\text{Al}_2\text{O}_3$  (16.7 wt%). It was found that under the thermodynamic driving force and the pressure driving force scenarios, the energy capacity of the system was maintained at 64% after 10 cycles. The decrease in capacity may be partly attributable to the excessive heating in the reactor bed leading to the massive formation of  $\text{Ca}_{12}\text{Al}_{14}\text{O}_{33}$ .

### 5.3. Other CaO-Based Composites

Lu et al. [137] loaded  $\text{Li}_2\text{SO}_4$  onto nano- $\text{CaCO}_3$  by the wet impregnation method. The results showed that after 11 cycles, the CaO conversion of the composite loaded with 5 wt%  $\text{Li}_2\text{SO}_4$  was 51%, which was 87% higher than that of pure nano- $\text{CaO}$  material. Additionally, both the carbonation and calcination reaction rates were improved, and the decomposition temperature was reduced by at least  $15^\circ\text{C}$ . Sarrion et al. [109] prepared  $\text{CaO}/\text{ZrO}_2$  composites by the mechanical mixing method. However, the improvement of  $\text{ZrO}_2$  on the heat storage performance of the doped sample was not obvious. The effective conversion of  $\text{CaO}/\text{ZrO}_2$  composites with 5%  $\text{ZrO}_2$  dropped to below 0.25 after 10 cycles. Khosa et al. [138] doped  $\text{ZnO}$  into  $\text{CaCO}_3$  by the mechanical mixing method and found that the heat storage material with 5 wt.%  $\text{ZnO}$  showed the highest heat storage capacity of 1478.8 kJ/kg. As the cycle number increased from 20 to 100, the heat storage density did not decrease, and the specific heat capacity of the sample doped with  $\text{ZnO}$  increased by 68%. They also studied the kinetics of the calcination reaction and found that the incorporation of  $\text{ZnO}$  could increase the rate of the calcination reaction. Xu et al. [139] prepared  $\text{CaO}/\text{TiO}_2$  composites by the stirring and mixing method and examined heat storage capacities of the composites in a synchronous thermal analyzer (STA) and a fixed-bed reactor. They found that the heat storage density of the composite containing 2.5 mol%  $\text{TiO}_2$  was 798.37 kJ/kg after 30 cycles, which was 2.26 times as high as that of the pure  $\text{CaCO}_3$  sample. This indicated that  $\text{CaO}/\text{TiO}_2$  composite had better sintering resistance.

### 5.4. Organic Acid-Treated CaO-Based Composites

Pretreatment of natural calcium-based materials with organic acids can improve the pore structures of the materials, which enhances heat storage performance. Sánchez-Jiménez et al. [140] treated a mixture of limestone and dolomite with acetic acid to prepare calcium magnesium acetate ( $\text{CaMgAc}$ ) material.  $\text{CaMgAc}$  possessed a stable porous structure, and nano- $\text{MgO}$  grains were uniformly dispersed around  $\text{CaO}$ , which improved the sintering resistance of  $\text{CaO}$ . The effects of the acetic acid treatment on the heat storage characteristics of limestone are exhibited in Figure 10a. After 30 energy storage cycles, the effective conversion of natural limestone was only 0.38, while that of modified limestone with acetic acid was as high as 0.56. In addition, the effective conversion of  $\text{CaMg50Ac}$  after 30 cycles was 0.70, which was much higher than that of limestone, as shown in Figure 10b.

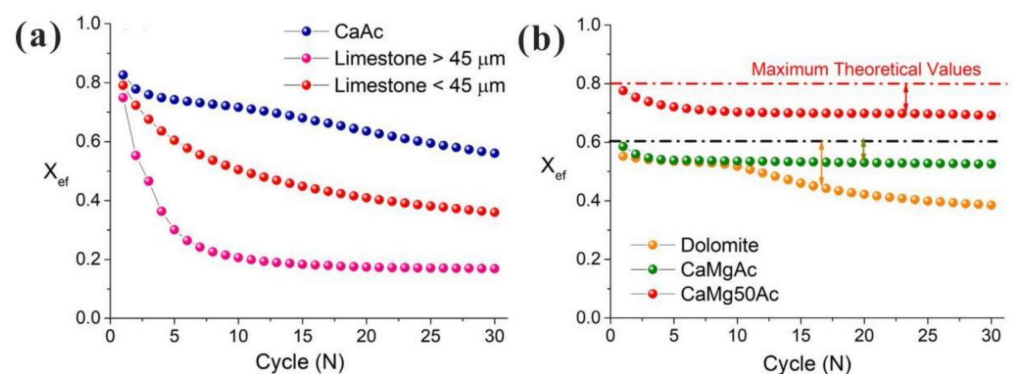


**Figure 10.** Cyclic effective conversions of CaO-based materials [140]: (a) limestone, CaAc; (b) dolomite, CaMgAc, and CaMg50Ac.

Wang et al. [34] used citric acid, with stronger acidity and of lower price, to treat limestone and dolomite to prepare  $\text{CaO}/\text{MgO}$  composite materials. When the molar ratio of  $\text{Ca}^{2+}/\text{citric acid}/\text{Mg}^{2+}$  was 8:7:1, the composite exhibited higher storage cyclic stability in the heat storage cycles. Thermal storage density of the composite achieved 2450 kJ/kg after 20 cycles. Han et al. [141] prepared  $\text{Ca}/\text{Al}$  composite heat storage materials with four different calcium-based precursors (calcium formate, calcium acetate, calcium lactate, calcium gluconate), aluminum acetylacetonate, and citric acid. They found that the  $\text{Ca}/\text{Al}$

composite with the molar ratio of Ca to Al = 9:1 exhibited the largest volumetric heat storage density of 2.35 GJ/m<sup>3</sup>, which only dropped by 12% after 20 cycles.

## 6. Improvement on Optical and Thermal Properties of CaO-Based Materials in CaO/CaCO<sub>3</sub> TCHS

The Tammann temperature of calcium-based materials is relatively low, so CaO grains agglomerate and grow up during cyclic heat storage process at high temperature, leading to the blockage of the pore structure, which is manifested as a gradual decline in heat storage performance [43,123]. A large number of researches have focused on slowing down the sintering speed of calcium-based heat storage materials to improve cyclic stability. As mentioned in Section 3.2, the volumetric heat collection is more suitable for CaO/CaCO<sub>3</sub> heat storage system, which requires calcium-based materials with great optical and thermal properties. However, natural calcium-based materials usually have poor optical absorption capacities and thermal conductivity. In recent years, the optical absorption capacity and thermal conductivity of natural calcium-based materials have been given more attention and represent a valuable research direction.

Han et al. [142] prepared composite materials by impregnating in H<sub>3</sub>BO<sub>3</sub> solution with CaCO<sub>3</sub> and adding expanded graphite with high thermal conductivity for heat storage. They found that the thermal conductivity of the composite materials increased by 60% when 3 wt% expanded graphite was added. The expanded graphite exhibited strong sintering resistance. The heat storage density of the composite material was 1313 kJ/kg after 50 cycles, while that of limestone was only 452 kJ/kg. On this basis, Han et al. [143] also studied an effective compression method to make graphite nanosheets better support the pore structure of CaO-based materials, so the obtained composites possessed a higher volumetric energy density. However, it is worth noting that CO<sub>2</sub> attaches to graphite at high temperatures to form CO gas. More consideration should be given when choosing graphite as an additive. Da et al. [79] put forward a new idea to increase the blackness of calcium-based materials to achieve the direct absorption of solar energy in a CaO/CaCO<sub>3</sub> heat storage system. Their experiments showed that adding black FeMnO<sub>3</sub> and Fe<sub>2</sub>O<sub>3</sub> to CaO by the sol-gel method improved the optical absorption properties of the materials. When the molar ratio of Ca/Mn/Fe was 100:4:8, the solar absorption of the composite reached 89.81% as exhibited in Figure 11. In addition, the existence of FeMnO<sub>3</sub> and Fe<sub>2</sub>O<sub>3</sub> also enhanced the sintering resistance of CaO. The effective conversion of Ca/Fe/Mn composites remained as high as 0.8 after 20 cycles.

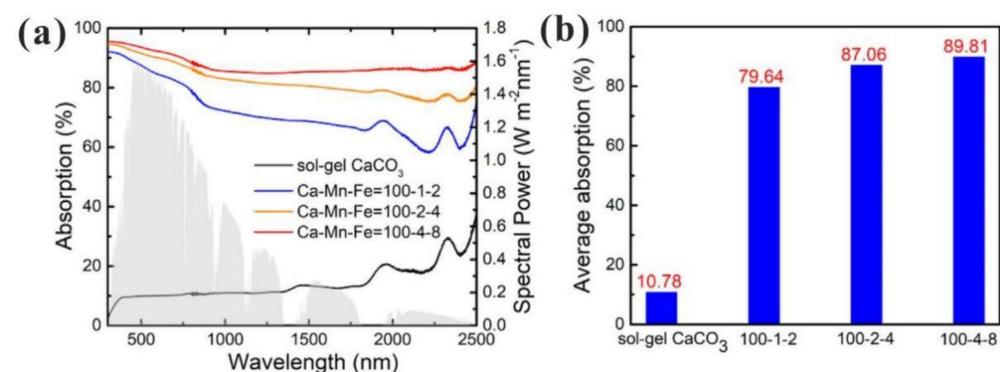


Figure 11. Optical absorption properties of CaO-based composites [79]: (a) Spectrum; (b) Absorption.

Moreover, Teng et al. [82] optimized the structure of the Ca/Fe/Mn composite by using calcium gluconate as the precursor to prepare a porous Ca/Fe/Mn composite with an optical absorption rate of 90%. The heat storage capacity of the Ca/Fe/Mn composite decreased by 3.31% in 60 cycles. The average heat storage density of the composite after 60 cycles was 1450 kJ/kg, which was 1.76 times as high as that of CaCO<sub>3</sub>, indicating that it had higher cyclic stability. Song et al. [144] used aluminum nitrate and iron nitrate as precursors to dope iron and aluminum into CaCO<sub>3</sub> powder by the sol-gel method. They

found that the decomposition rate of the composite increased and the decomposition temperature decreased. After 50 cycles, the heat storage density of the composite only dropped by 4.5%, which was about 87% higher than that of pure  $\text{CaCO}_3$ . Similarly, the average optical absorption rate of the composite achieved 45.6%, while that of pure  $\text{CaCO}_3$  reached only 8%. Li et al. [145] used  $\text{Ca}(\text{OH})_2$  powder,  $\text{MnC}_4\text{H}_6\text{O}_4 \cdot 4\text{H}_2\text{O}$  and SiC by extrusion-spheronization method to prepare Mn/SiC doped CaO pellets. They found that when SiC and  $\text{MnO}_2$  were both doped at 5 wt%, CaO pellets exhibited the highest the optical absorption and heat storage capacity. In addition, the effective conversion of the Mn/SiC doped CaO pellets remained 0.48 after 30 cycles, while that of the pure CaO pellets achieved only 0.34. Similarly, the average optical absorption of the Mn/SiC doped CaO pellets reached 53%, while that of the original CaO particles was only 3%. Yang et al. [146] prepared Ca/Fe/Mn composite heat storage materials by utilizing carbonaceous microspheres as templates, which mainly consisted of  $\text{CaCO}_3$  and  $\text{Ca}_2\text{FeMnO}_5$ . The average spectral absorption rate of the synthetic material with the molar ratio of Ca/Fe/Mn = 100:2:7 reached 76.8%, while that of pure  $\text{CaCO}_3$  was only 10.8%. Zheng et al. [147] examined a variety of dark composite calcium-based heat storage materials by the sol-gel method, including Ca/Cu, Ca/Cu/Fe, Ca/Cu/Co, Ca/Cu/Cr, Ca/Cu/Mn, and Ca/Al/Cu/Fe materials. The results showed that Ca/Cu/Co, Ca/Cu/Cr, and Ca/Cu/Mn materials had strong optical absorption capacities, and their average spectral absorption of solar energy was greater than 60%.

Table 4 summarizes the heat storage properties of the different CaO-based materials reported in the literature. It is found that adding dopants is still the most effective and common method to improve the heat storage stability of CaO-based materials. However, it is still unavoidable that the activity of CaO-based material decreases during long-term heat storage cycles. Calcium-based materials often need to add enough supporters to maintain relatively stable heat storage performance. This also decreases the content of CaO in the calcium-based material, resulting in a decrease in the heat storage density of the material per unit mass. Thus, how to enhance the heat storage performance and cyclic stability of calcium-based materials remain important. In addition, how to improve the optical and thermal properties of CaO-based materials is also the focus of researchers.

**Table 4.** Comparison of heat storage properties of CaO-based materials reported in the literature.

| Additives                               | Doping Ratio (wt%) | Carbonation Pressure (bar) | Cycles | Effective Conversion | Reference |
|---|--------------------|----------------------------|--------|----------------------|-----------|
| $\text{SiO}_2$                          | 10%                | 1                          | 20     | 0.30                 | [126]     |
| $\text{SiO}_2$                          | 30%                | 1                          | 20     | 0.34                 | [126]     |
| $\text{SiO}_2$                          | 5%                 | 1                          | 20     | 0.20                 | [127]     |
| $\text{SiO}_2$                          | 37.5%              | 1                          | 45     | 0.20                 | [129]     |
| $\text{SiO}_2$                          | 20%                | 5                          | 50     | 0.29                 | [130]     |
| $\text{Al}_2\text{O}_3$                 | 20%                | 5                          | 50     | 0.62                 | [130]     |
| $\text{Al}_2\text{O}_3$                 | 5%                 | 1                          | 20     | 0.55                 | [131]     |
| $\text{ZrO}_2$                          | 5%                 | 1                          | 10     | 0.22                 | [109]     |
| $\text{ZrO}_2$                          | 20%                | 5                          | 50     | 0.67                 | [130]     |
| $\text{ZrO}_2$                          | 40%                | 5                          | 50     | 0.45                 | [130]     |
| ZnO                                     | 20%                | 5                          | 50     | 0.07                 | [130]     |
| $\text{Fe}_2\text{O}_3$                 | 20%                | 5                          | 50     | 0.08                 | [130]     |
| Ni                                      | 20%                | 5                          | 50     | 0.14                 | [130]     |
| $\text{BaCO}_3$                         | 9.5%               | 5                          | 50     | 0.09                 | [130]     |
| $\text{Li}_2\text{SO}_4$                | 5%                 | 1                          | 11     | 0.48                 | [137]     |
| $\text{Al}_2\text{O}_3/\text{CeO}_2$    | 5%/5%              | 13                         | 30     | 0.79                 | [136]     |
| Graphite                                | 20%                | 5                          | 50     | 0.25                 | [130]     |
| $\text{H}_3\text{BO}_3/\text{Graphite}$ | 3%                 | 1                          | 50     | 0.41                 | [142]     |
| Mn/Fe                                   | -                  | 1                          | 20     | 0.80                 | [79]      |
| Al/Citric acid                          | -                  | 1                          | 20     | 0.7                  | [133]     |
| Acetic acid(Ac)                         | -                  | 1                          | 30     | 0.56                 | [140]     |
| Mg/Ac                                   | -                  | 1                          | 30     | 0.70                 | [140]     |
| NaY                                     | 20%                | 5                          | 50     | 0.23                 | [130]     |
| HY                                      | 20%                | 5                          | 50     | 0.16                 | [130]     |
| Mor                                     | 20%                | 5                          | 50     | 0.15                 | [130]     |

## 7. Conclusions

This paper reviewed and summarized the research progress of CaO/CaCO<sub>3</sub> heat storage in terms of system design, reaction conditions, and material properties. By summarizing a variety of integration schemes for CaO/CaCO<sub>3</sub> heat storage and CSP plants, the closed CO<sub>2</sub> Brayton cycle heat storage system is the most ideal integrated scheme. The performance degradation of CaO-based materials is still a major problem that restricts the development of CaO/CaCO<sub>3</sub> heat storage technology. The potential future research works are shown as follows:

- (1) System integration is currently limited to simulation research, which faces technological challenges, such as the fluctuation of solar radiation, the separation of gas-solid two phases, and so on, to realize industrial applications. The integrated system of CaO/CaCO<sub>3</sub> heat storage and CSP plant should be further designed and optimized to improve the sensible heat recovery network of the system and reduce energy loss. The design and production of equipment that is more compatible with CaO/CaCO<sub>3</sub> heat storage, especially particle receivers, need to meet the main requirements of great scalability and high thermal efficiency.
- (2) The preparation of CaO-based heat storage materials should be carried out in the direction of high cyclic activity and cyclic stability, and the preparation process of the materials should be optimized. The ideal CaO-based heat storage materials possess high heat storage density, great heat storage stability, and great absorption of sunlight, while economical preparation processes are also required. In addition, the specific application of the material needs to be combined with the reactor design.

**Author Contributions:** Conceptualization, Y.Y.; methodology, Y.L.; validation, X.Y.; formal analysis, C.Z.; investigation, J.Z.; writing—original draft preparation, Y.Y.; writing—review and editing, Y.L.; project administration, Y.L. and J.Z. All authors have read and agreed to the published version of the manuscript.

**Funding:** This research was funded by Shandong Provincial Natural Science Foundation (grant number: ZR2020ME188).

**Institutional Review Board Statement:** Not applicable.

**Informed Consent Statement:** Not applicable.

**Data Availability Statement:** Not applicable.

**Acknowledgments:** Authors appreciate the copyright holder: © Elsevier B.V.

**Conflicts of Interest:** The authors declare no conflict of interest. The funders had no role in the design of the study; in the collection, analyses, or interpretation of data; in the writing of the manuscript, or in the decision to publish the results.

## References

1. Oyekale, J.; Petrollese, M.; Tola, V.; Cau, G. Impacts of Renewable Energy Resources on Effectiveness of Grid-Integrated Systems: Succinct Review of Current Challenges and Potential Solution Strategies. *Energies* **2020**, *13*, 4856. [[CrossRef](#)]
2. Masson-Delmotte, V.; Zhai, P.; Pörtner, H.-O.; Roberts, D.; Skea, J.; Shukla, P.R.; Pirani, A.; Moufouma-Okia, W.; Péan, C.; Pidcock, R. *Global Warming of 1.5 °C. An IPCC Special Report on the Impacts of Global Warming*; Intergovernmental Panel on Climate Change: Geneva, Switzerland, 2018; Volume 1, pp. 1–9.
3. Dudley, B. *BP Energy Outlook. Report—BP Energy Economics*; B.P.: London, UK, 2019; Volume 9.
4. Li, J.; Liu, J.; Yan, P.; Li, X.; Zhou, G.; Yu, D. Operation Optimization of Integrated Energy System under a Renewable Energy Dominated Future Scene Considering Both Independence and Benefit: A Review. *Energies* **2021**, *14*, 1103. [[CrossRef](#)]
5. Bravo, R.; Ortiz, C.; Chacartegui, R.; Friedrich, D. Hybrid solar power plant with thermochemical energy storage: A multi-objective operational optimisation. *Energy Convers. Manag.* **2020**, *205*, 112421. [[CrossRef](#)]
6. del Río, P.; Peñasco, C.; Mir-Artigues, P. An overview of drivers and barriers to concentrated solar power in the European Union. *Renew. Sustain. Energy Rev.* **2018**, *81*, 1019–1029. [[CrossRef](#)]
7. Peng, X.; Root, T.W.; Maravelias, C.T. Storing solar energy with chemistry: The role of thermochemical storage in concentrating solar power. *Green Chem.* **2017**, *19*, 2427–2438. [[CrossRef](#)]

8. Ellingwood, K.; Mohammadi, K.; Powell, K. A novel means to flexibly operate a hybrid concentrated solar power plant and improve operation during non-ideal direct normal irradiation conditions. *Energy Convers. Manag.* **2020**, *203*, 112275. [[CrossRef](#)]
9. Ortiz, C.; Binotti, M.; Romano, M.C.; Valverde, J.M.; Chacartegui, R. Off-design model of concentrating solar power plant with thermochemical energy storage based on calcium-looping. *AIP Conf. Proc.* **2019**, *2126*, 210006.
10. Heuberger, C.F.; Mac Dowell, N. Real-World Challenges with a Rapid Transition to 100% Renewable Power Systems. *Joule* **2018**, *2*, 367–370. [[CrossRef](#)]
11. Chang, C. Tracking solar collection technologies for solar heating and cooling systems. In *Advances in Solar Heating and Cooling*; Elsevier: Amsterdam, The Netherlands, 2016; pp. 81–93.
12. Kuravi, S.; Trahan, J.; Goswami, D.Y.; Rahman, M.M.; Stefanakos, E.K. Thermal energy storage technologies and systems for concentrating solar power plants. *Prog. Energy Combust. Sci.* **2013**, *39*, 285–319. [[CrossRef](#)]
13. Pelay, U.; Luo, L.; Fan, Y.; Stitou, D.; Rood, M. Thermal energy storage systems for concentrated solar power plants. *Renew. Sustain. Energy Rev.* **2017**, *79*, 82–100. [[CrossRef](#)]
14. Fernandez, A.I.; Martínez, M.; Segarra, M.; Martorell, I.; Cabeza, L.F. Selection of materials with potential in sensible thermal energy storage. *Sol. Energy Mater. Sol. Cells* **2010**, *94*, 1723–1729. [[CrossRef](#)]
15. Riffat, S.; Mempo, B.; Fang, W. Phase change material developments: A review. *Int. J. Ambient Energy* **2015**, *36*, 102–115. [[CrossRef](#)]
16. Regin, A.F.; Solanki, S.C.; Saini, J.S. Heat transfer characteristics of thermal energy storage system using PCM capsules: A review. *Renew. Sustain. Energy Rev.* **2008**, *12*, 2438–2458. [[CrossRef](#)]
17. Abedin, A.H.; Rosen, M.A. Closed and open thermochemical energy storage: Energy-and exergy-based comparisons. *Energy* **2012**, *41*, 83–92. [[CrossRef](#)]
18. Wei, L.; Wei, C.; Dandan, W. Research and development of thermochemical energy storage based on hydrated salt. *Refrig. Air-Cond.* **2017**, *17*, 14–21.
19. Yan, T.; Wang, R.; Li, T.; Wang, L.; Fred, I.T. A review of promising candidate reactions for chemical heat storage. *Renew. Sustain. Energy Rev.* **2015**, *43*, 13–31. [[CrossRef](#)]
20. Pardo, P.; Deydier, A.; Anxionnaz-Minvielle, Z.; Rougé, S.; Cabassud, M.; Cognet, P. A review on high temperature thermochemical heat energy storage. *Renew. Sustain. Energy Rev.* **2014**, *32*, 591–610. [[CrossRef](#)]
21. Ma, Z.; Wu, S.; Li, Y. Research progress of CO<sub>2</sub> capture with the assist CaO-based energy storage materials at coal-fired power station. *Clean Coal Technol.* **2019**, *25*, 1–8.
22. Mahon, D.; Claudio, G.; Eames, P. An Experimental Study of the Decomposition and Carbonation of Magnesium Carbonate for Medium Temperature Thermochemical Energy Storage. *Energies* **2021**, *14*, 1316. [[CrossRef](#)]
23. Rhodes, N.R.; Barde, A.; Randhir, K.; Li, L.; Hahn, D.W.; Mei, R.; Klausner, J.F.; AuYeung, N.J. Solar Thermochemical Energy Storage Through Carbonation Cycles of SrCO<sub>3</sub>/SrO Supported on SrZrO<sub>3</sub>. *ChemSusChem* **2015**, *8*, 3793–3798. [[CrossRef](#)]
24. Criado, Y.; Alonso, M.; Abanades, J.; Anxionnaz-Minvielle, Z. Conceptual process design of a CaO/Ca(OH)<sub>2</sub> thermochemical energy storage system using fluidized bed reactors. *Appl. Therm. Eng.* **2014**, *73*, 1087–1094. [[CrossRef](#)]
25. Seitz, G. Modeling fixed-bed reactors for thermochemical heat storage with the reaction system CaO/Ca(OH)<sub>2</sub>. *Appl. Sci.* **2021**, *11*, 682. [[CrossRef](#)]
26. Nyallang Nyamsi, S.; Tolj, I.; Lototsky, M. Metal hydride beds-phase change materials: Dual mode thermal energy storage for medium-high temperature industrial waste heat recovery. *Energies* **2019**, *12*, 3949. [[CrossRef](#)]
27. Preisner, N.C.; Linder, M. A moving bed reactor for thermochemical energy storage based on metal oxides. *Energies* **2020**, *13*, 1232. [[CrossRef](#)]
28. Müller, D.; Knoll, C.; Gravogl, G.; Jordan, C.; Eitenberger, E.; Friedbacher, G.; Artner, W.; Welch, J.M.; Werner, A.; Harasek, M. Medium-temperature thermochemical energy storage with transition metal ammoniates—A systematic material comparison. *Appl. Energy* **2021**, *285*, 116470. [[CrossRef](#)]
29. Li, W.; Hao, Y. Efficient solar power generation combining photovoltaics and mid-/low-temperature methanol thermochemistry. *Appl. Energy* **2017**, *202*, 377–385. [[CrossRef](#)]
30. Wong, B.; Brown, L.; Buckingham, R.; Sweet, W.; Russ, B.; Gorenssek, M. Sulfur dioxide disproportionation for sulfur based thermochemical energy storage. *Sol. Energy* **2015**, *118*, 134–144. [[CrossRef](#)]
31. Sunku Prasad, J.; Muthukumar, P.; Desai, F.; Basu, D.N.; Rahman, M.M. A critical review of high-temperature reversible thermochemical energy storage systems. *Appl. Energy* **2019**, *254*, 113733. [[CrossRef](#)]
32. Ortiz, C.; Valverde, J.M.; Chacartegui, R.; Perez-Maqueda, L.A.; Giménez, P. The Calcium-Looping (CaCO<sub>3</sub>/CaO) process for thermochemical energy storage in Concentrating Solar Power plants. *Renew. Sustain. Energy Rev.* **2019**, *113*, 109252. [[CrossRef](#)]
33. Abedin, A.H.; Rosen, M.A. A critical review of thermochemical energy storage systems. *Open Renew. Energy J.* **2011**, *4*, 42–46. [[CrossRef](#)]
34. Wang, K.; Gu, F.; Clough, P.T.; Zhao, P.; Anthony, E.J. Porous MgO-stabilized CaO-based powders/pellets via a citric acid-based carbon template for thermochemical energy storage in concentrated solar power plants. *Chem. Eng. J.* **2020**, *390*, 124163. [[CrossRef](#)]
35. Barin, I.; Platzki, G. *Thermochemical Data of Pure Substances*; Wiley Online Library: Hoboken, NJ, USA, 1989; Volume 304.
36. Ortiz, C.; Chacartegui, R.; Valverde, J.; Alovio, A.; Becerra, J. Power cycles integration in concentrated solar power plants with energy storage based on calcium looping. *Energy Convers. Manag.* **2017**, *149*, 815–829. [[CrossRef](#)]

37. Kyaw, K.; Kubota, M.; Watanabe, F.; Matsuda, H.; Hasatani, M. Study of carbonation of CaO for high temperature thermal energy storage. *J. Chem. Eng. Jpn.* **1998**, *31*, 281–284. [[CrossRef](#)]
38. Cormos, C.-C. Economic evaluations of coal-based combustion and gasification power plants with post-combustion CO<sub>2</sub> capture using calcium looping cycle. *Energy* **2014**, *78*, 665–673. [[CrossRef](#)]
39. Zsembinski, G.; Solé, A.; Barreneche, C.; Prieto, C.; Fernández, A.I.; Cabeza, L.F. Review of reactors with potential use in thermochemical energy storage in concentrated solar power plants. *Energies* **2018**, *11*, 2358. [[CrossRef](#)]
40. Yuan, Y.; Li, Y.; Zhao, J. Development on Thermochemical Energy Storage Based on CaO-Based Materials: A Review. *Sustainability* **2018**, *10*, 2660. [[CrossRef](#)]
41. Felderhoff, M.; Urbanczyk, R.; Peil, S. Thermochemical heat storage for high temperature applications—A review. *Green* **2013**, *3*, 113–123. [[CrossRef](#)]
42. Wentworth, W.; Chen, E. Simple thermal decomposition reactions for storage of solar thermal energy. *Sol. Energy* **1976**, *18*, 205–214. [[CrossRef](#)]
43. Chen, J.; Duan, L.; Sun, Z. Review on the Development of Sorbents for Calcium Looping. *Energy Fuels* **2020**, *34*, 7806–7836. [[CrossRef](#)]
44. Fedunik-Hofman, L.; Bayon, A.; Donne, S.W. Comparative kinetic analysis of CaCO<sub>3</sub>/CaO reaction system for energy storage and carbon capture. *Appl. Sci.* **2019**, *9*, 4601. [[CrossRef](#)]
45. Valverde, J.M. The Ca-looping process for CO<sub>2</sub> capture and energy storage: Role of nanoparticle technology. *J. Nanoparticle Res.* **2018**, *20*, 1–16. [[CrossRef](#)]
46. Chen, J.; Duan, L.; Sun, Z. Accurate control of cage-like CaO hollow microspheres for enhanced CO<sub>2</sub> capture in calcium looping via a template-assisted synthesis approach. *Environ. Sci. Technol.* **2019**, *53*, 2249–2259. [[CrossRef](#)] [[PubMed](#)]
47. He, D.; Ou, Z.; Qin, C.; Deng, T.; Yin, J.; Pu, G. Understanding the catalytic acceleration effect of steam on CaCO<sub>3</sub> decomposition by density function theory. *Chem. Eng. J.* **2020**, *379*, 122348. [[CrossRef](#)]
48. Martínez, I.; Grasa, G.; Murillo, R.; Arias, B.; Abanades, J. Modelling the continuous calcination of CaCO<sub>3</sub> in a Ca-looping system. *Chem. Eng. J.* **2013**, *215*, 174–181. [[CrossRef](#)]
49. Ortiz, C.; Valverde, J.M.; Chacartegui, R.; Perez-Maqueda, L.A. Carbonation of Limestone Derived CaO for Thermochemical Energy Storage: From Kinetics to Process Integration in Concentrating Solar Plants. *ACS Sustain. Chem. Eng.* **2018**, *6*, 6404–6417. [[CrossRef](#)]
50. Borgwardt, R.H. Sintering of nascent calcium oxide. *Chem. Eng. Sci.* **1989**, *44*, 53–60. [[CrossRef](#)]
51. Bazaikin, Y.V.; Malkovich, E.; Derevschikov, V.; Lysikov, A.; Okunev, A. Evolution of sorptive and textural properties of CaO-based sorbents during repetitive sorption/regeneration cycles. *Chem. Eng. Sci.* **2016**, *152*, 709–716. [[CrossRef](#)]
52. Sarrion, B.; Valverde, J.M.; Perejon, A.; Perez-Maqueda, L.; Sanchez-Jimenez, P.E. On the Multicycle Activity of Natural Limestone/Dolomite for Thermochemical Energy Storage of Concentrated Solar Power. *Energy Technol.* **2016**, *4*, 1013–1019. [[CrossRef](#)]
53. Avila-Marin, A.L. Volumetric receivers in solar thermal power plants with central receiver system technology: A review. *Sol. Energy* **2011**, *85*, 891–910. [[CrossRef](#)]
54. Reich, L.; Melmoth, L.; Yue, L.; Bader, R.; Gresham, R.; Simon, T.; Lipiński, W. A solar reactor design for research on calcium oxide-based carbon dioxide capture. *J. Sol. Energy Eng.* **2017**, *139*, 054501. [[CrossRef](#)]
55. Valverde, J.M.; Medina, S. Crystallographic transformation of limestone during calcination under CO<sub>2</sub>. *Phys. Chem. Chem. Phys.* **2015**, *17*, 21912–21926. [[CrossRef](#)] [[PubMed](#)]
56. Charitos, A.; Rodríguez, N.; Hawthorne, C.; Alonso, M.; Zieba, M.; Arias, B.; Kopanakis, G.; Scheffknecht, G.n.; Abanades, J.C. Experimental validation of the calcium looping CO<sub>2</sub> capture process with two circulating fluidized bed carbonator reactors. *Ind. Eng. Chem. Res.* **2011**, *50*, 9685–9695. [[CrossRef](#)]
57. Arcenegui-Troya, J.; Sánchez-Jiménez, P.E.; Perejón, A.; Moreno, V.; Valverde, J.M.; Pérez-Maqueda, L.A. Kinetics and cyclability of limestone (CaCO<sub>3</sub>) in presence of steam during calcination in the CaL scheme for thermochemical energy storage. *Chem. Eng. J.* **2021**, *417*, 129194. [[CrossRef](#)]
58. Khosa, A.A.; Xu, T.; Xia, B.Q.; Yan, J.; Zhao, C.Y. Technological challenges and industrial applications of CaCO<sub>3</sub>/CaO based thermal energy storage system—A review. *Sol. Energy* **2019**, *193*, 618–636. [[CrossRef](#)]
59. Lanchi, M.; Turchetti, L.; Sau, S.; Liberatore, R.; Cerbelli, S.; Murmura, M.A.; Annesini, M.C. A Discussion of Possible Approaches to the Integration of Thermochemical Storage Systems in Concentrating Solar Power Plants. *Energies* **2020**, *13*, 4940. [[CrossRef](#)]
60. Chang, M.-H.; Chen, W.-C.; Huang, C.-M.; Liu, W.-H.; Chou, Y.-C.; Chang, W.-C.; Chen, W.; Cheng, J.-Y.; Huang, K.-E.; Hsu, H.-W. Design and experimental testing of a 1.9 MWth calcium looping pilot plant. *Energy Procedia* **2014**, *63*, 2100–2108. [[CrossRef](#)]
61. Valverde, J.M.; Barea-López, M.; Perejón, A.; Sánchez-Jiménez, P.E.; Pérez-Maqueda, L.A. Effect of Thermal Pretreatment and Nanosilica Addition on Limestone Performance at Calcium-Looping Conditions for Thermochemical Energy Storage of Concentrated Solar Power. *Energy Fuels* **2017**, *31*, 4226–4236. [[CrossRef](#)]
62. Edwards, S.E.B.; Materić, V. Calcium looping in solar power generation plants. *Sol. Energy* **2012**, *86*, 2494–2503. [[CrossRef](#)]
63. Chacartegui, R.; Alovísio, A.; Ortiz, C.; Valverde, J.M.; Verda, V.; Becerra, J.A. Thermochemical energy storage of concentrated solar power by integration of the calcium looping process and a CO<sub>2</sub> power cycle. *Appl. Energy* **2016**, *173*, 589–605. [[CrossRef](#)]
64. Alovísio, A.; Chacartegui, R.; Ortiz, C.; Valverde, J.M.; Verda, V. Optimizing the CSP-Calcium Looping integration for Thermochemical Energy Storage. *Energy Convers. Manag.* **2017**, *136*, 85–98. [[CrossRef](#)]

65. Karasavvas, E.; Panopoulos, K.D.; Papadopoulou, S.; Voutetakis, S. Design of an integrated CSP-calcium looping for uninterrupted power production through energy storage. *Chem. Eng. Trans.* **2018**, *70*, 2131–2136.
66. Tesio, U.; Guelpa, E.; Verda, V. Optimal Indirect Integration of Steam Rankine Cycles in Concentrated Solar Power Coupled with Thermochemical Storage. *E3S Web Conf.* **2020**, *197*, 01005. [[CrossRef](#)]
67. Ortiz, C.; Romano, M.C.; Valverde, J.M.; Binotti, M.; Chacartegui, R. Process integration of Calcium-Looping thermochemical energy storage system in concentrating solar power plants. *Energy* **2018**, *155*, 535–551. [[CrossRef](#)]
68. Karasavvas, E.; Panopoulos, K.D.; Papadopoulou, S.; Voutetakis, S. Energy and exergy analysis of the integration of concentrated solar power with calcium looping for power production and thermochemical energy storage. *Renew. Energy* **2020**, *154*, 743–753. [[CrossRef](#)]
69. Cannone, S.F.; Stendardo, S.; Lanzini, A. Solar-Powered Rankine Cycle Assisted by an Innovative Calcium Looping Process as an Energy Storage System. *Ind. Eng. Chem. Res.* **2020**, *59*, 6977–6993. [[CrossRef](#)]
70. Wu, S.; Zhou, C.; Tremain, P.; Doroodchi, E.; Moghtaderi, B. A phase change calcium looping thermochemical energy storage system based on  $\text{CaCO}_3/\text{CaO}-\text{CaCl}_2$ . *Energy Convers. Manag.* **2021**, *227*, 113503. [[CrossRef](#)]
71. Habibi, R.; Mehrpooya, M.; Pourmoghadam, P. Integrated Mg-Cl hydrogen production process and  $\text{CaO}/\text{CaCO}_3-\text{CaCl}_2$  thermochemical energy storage phase change system using solar tower system. *Energy Convers. Manag.* **2021**, *245*, 114555. [[CrossRef](#)]
72. Chen, X.; Zhang, D.; Wang, Y.; Ling, X.; Jin, X. The role of sensible heat in a concentrated solar power plant with thermochemical energy storage. *Energy Convers. Manag.* **2019**, *190*, 42–53. [[CrossRef](#)]
73. Pascual, S.; Lisbona, P.; Bailera, M.; Romeo, L.M. Design and operational performance maps of calcium looping thermochemical energy storage for concentrating solar power plants. *Energy* **2021**, *220*, 119715. [[CrossRef](#)]
74. Peng, X.; Yao, M.; Root, T.W.; Maravelias, C.T. Design and analysis of concentrating solar power plants with fixed-bed reactors for thermochemical energy storage. *Appl. Energy* **2020**, *262*, 114543. [[CrossRef](#)]
75. Obermeier, J.; Müller, K.; Karagiannakis, G.; Stubos, A.; Arlt, W. A novel thermochemical energy storage and transportation concept based on concentrated solar irradiation-aided  $\text{CaO}$ -looping. *AIP Conf. Proc.* **2016**, *1734*, 050033.
76. Flamant, G.; Benoit, H.; Jenke, M.; Santos, A.F.; Tescari, S.; Moumin, G.; Rodriguez, A.; Azapagic, A.; Stamford, L.; Baeyens, J. Solar processing of reactive particles up to 900 °C, the SOLPART project. *AIP Conf. Proc.* **2018**, *2033*, 20004.
77. Sun, J.; Sun, Y.; Yang, Y.; Tong, X.; Liu, W. Plastic/rubber waste-templated carbide slag pellets for regenerable  $\text{CO}_2$  capture at elevated temperature. *Appl. Energy* **2019**, *242*, 919–930. [[CrossRef](#)]
78. Flamant, G.; Hernandez, D.; Bonet, C.; Traverse, J.-P. Experimental aspects of the thermochemical conversion of solar energy; Decarbonation of  $\text{CaCO}_3$ . *Sol. Energy* **1980**, *24*, 385–395. [[CrossRef](#)]
79. Da, Y.; Xuan, Y.; Teng, L.; Zhang, K.; Liu, X.; Ding, Y. Calcium-based composites for direct solar-thermal conversion and thermochemical energy storage. *Chem. Eng. J.* **2020**, *382*, 122815. [[CrossRef](#)]
80. Cuevas, A.; Martínez, L.; Romero, R.; Dalchiele, E.A.; Marotti, R.; Leinen, D.; Ramos-Barrado, J.R.; Martin, F. Electrochemically grown cobalt-alumina composite layer for solar thermal selective absorbers. *Sol. Energy Mater. Sol. Cells* **2014**, *130*, 380–386. [[CrossRef](#)]
81. Zeng, J.; Xuan, Y.; Duan, H. Tin-silica-silver composite nanoparticles for medium-to-high temperature volumetric absorption solar collectors. *Sol. Energy Mater. Sol. Cells* **2016**, *157*, 930–936. [[CrossRef](#)]
82. Teng, L.; Xuan, Y.; Da, Y.; Liu, X.; Ding, Y. Modified Ca-Looping materials for directly capturing solar energy and high-temperature storage. *Energy Storage Mater.* **2020**, *25*, 836–845. [[CrossRef](#)]
83. Lisbona, P.; Bailera, M.; Hills, T.; Sceats, M.; Díez, L.I.; Romeo, L.M. Energy consumption minimization for a solar lime calciner operating in a concentrated solar power plant for thermal energy storage. *Renew. Energy* **2020**, *156*, 1019–1027. [[CrossRef](#)]
84. Neises, M.; Tescari, S.; de Oliveira, L.; Roeb, M.; Sattler, C.; Wong, B. Solar-heated rotary kiln for thermochemical energy storage. *Sol. Energy* **2012**, *86*, 3040–3048. [[CrossRef](#)]
85. Bertocchi, R.; Karni, J.; Kribus, A. Experimental evaluation of a non-isothermal high temperature solar particle receiver. *Energy* **2004**, *29*, 687–700. [[CrossRef](#)]
86. Röger, M.; Amsbeck, L.; Gobereit, B.; Buck, R. Face-down solid particle receiver using recirculation. *J. Sol. Energy Eng.* **2011**, *133*. [[CrossRef](#)]
87. Tregambi, C.; Padula, S.; Galbusieri, M.; Coppola, G.; Montagnaro, F.; Salatino, P.; Troiano, M.; Solimene, R. Directly irradiated fluidized bed reactor for thermochemical energy storage and solar fuels production. *Powder Technol.* **2020**, *366*, 460–469. [[CrossRef](#)]
88. Yao, Y.; Wei, X.; Chen, L.; Li, S.; Tan, H. Research and application progress of the key technologies for high efficiency and low emission of cement kilns. *Clean Coal Technol.* **2020**, *26*, 1–10.
89. Moumin, G.; Tescari, S.; Sundarraj, P.; de Oliveira, L.; Roeb, M.; Sattler, C. Solar treatment of cohesive particles in a directly irradiated rotary kiln. *Sol. Energy* **2019**, *182*, 480–490. [[CrossRef](#)]
90. Alonso, E.; Romero, M. Review of experimental investigation on directly irradiated particles solar reactors. *Renew. Sustain. Energy Rev.* **2015**, *41*, 53–67. [[CrossRef](#)]
91. Yan, Y.; Wang, K.; Clough, P.T.; Anthony, E.J. Developments in calcium/chemical looping and metal oxide redox cycles for high-temperature thermochemical energy storage: A review. *Fuel Process. Technol.* **2020**, *199*, 106280. [[CrossRef](#)]
92. Hanak, D.P.; Manovic, V. Economic feasibility of calcium looping under uncertainty. *Appl. Energy* **2017**, *208*, 691–702. [[CrossRef](#)]
93. Michalski, S.; Hanak, D.P.; Manovic, V. Techno-economic feasibility assessment of calcium looping combustion using commercial technology appraisal tools. *J. Clean. Prod.* **2019**, *219*, 540–551. [[CrossRef](#)]

94. Bayon, A.; Bader, R.; Jafarian, M.; Fedunik-Hofman, L.; Sun, Y.; Hinkley, J.; Miller, S.; Lipiński, W. Techno-economic assessment of solid–gas thermochemical energy storage systems for solar thermal power applications. *Energy* **2018**, *149*, 473–484. [[CrossRef](#)]
95. Tesio, U.; Guelpa, E.; Verda, V. Integration of thermochemical energy storage in concentrated solar power. Part 1: Energy and economic analysis/optimization. *Energy Convers. Manag. X* **2020**, *6*, 100039. [[CrossRef](#)]
96. Muto, A.; McCabe, K.; Real, D. High-temperature calcium-based thermochemical energy storage system for use with CSP facilities. *AIP Conf. Proc.* **2018**, *2033*, 100006.
97. Benitez-Guerrero, M.; Sarrion, B.; Perejon, A.; Sanchez-Jimenez, P.E.; Perez-Maqueda, L.A.; Manuel Valverde, J. Large-scale high-temperature solar energy storage using natural minerals. *Sol. Energy Mater. Sol. Cells* **2017**, *168*, 14–21. [[CrossRef](#)]
98. Sun, H.; Li, Y.; Bian, Z.; Yan, X.; Wang, Z.; Liu, W. Thermochemical energy storage performances of Ca-based natural and waste materials under high pressure during CaO/CaCO<sub>3</sub> cycles. *Energy Convers. Manag.* **2019**, *197*, 111885. [[CrossRef](#)]
99. Chen, X.; Zhao, N.; Ling, X.; Wang, Y. Parameter analysis of discharging process for CaCO<sub>3</sub>/CaO thermochemical energy storage. *Energy Procedia* **2019**, *158*, 4617–4622. [[CrossRef](#)]
100. Fedunik-Hofman, L.; Bayon, A.; Hinkley, J.; Lipiński, W.; Donne, S.W. Friedman method kinetic analysis of CaO-based sorbent for high-temperature thermochemical energy storage. *Chem. Eng. Sci.* **2019**, *200*, 236–247. [[CrossRef](#)]
101. Barker, R. The reactivity of calcium oxide towards carbon dioxide and its use for energy storage. *J. Appl. Chem. Biotechnol.* **1974**, *24*, 221–227. [[CrossRef](#)]
102. Sarrión, B.; Perejón, A.; Sánchez-Jiménez, P.E.; Pérez-Maqueda, L.A.; Valverde, J.M. Role of calcium looping conditions on the performance of natural and synthetic Ca-based materials for energy storage. *J. CO<sub>2</sub> Util.* **2018**, *28*, 374–384. [[CrossRef](#)]
103. Tammann, G.; Westerhold, F.; Garre, B.; Kordes, E.; Kalsing, H. Chemische Reaktionen in pulverförmigen Gemengen zweier Kristallarten. *Z. Anorg. Allg. Chem.* **1925**, *149*, 21–98. [[CrossRef](#)]
104. Valverde, J.M.; Medina, S. Limestone calcination under calcium-looping conditions for CO<sub>2</sub> capture and thermochemical energy storage in the presence of H<sub>2</sub>O: An in situ XRD analysis. *Phys. Chem. Chem. Phys.* **2017**, *19*, 7587–7596. [[CrossRef](#)] [[PubMed](#)]
105. Sarrión, B.; Perejón, A.; Sánchez-Jiménez, P.E.; Amghar, N.; Chacartegui, R.; Valverde, J.M.; Pérez-Maqueda, L.A. Calcination under low CO<sub>2</sub> pressure enhances the calcium Looping performance of limestone for thermochemical energy storage. *Chem. Eng. J.* **2021**, *417*, 127922. [[CrossRef](#)]
106. Champagne, S.; Lu, D.Y.; Macchi, A.; Symonds, R.T.; Anthony, E.J. Influence of steam injection during calcination on the reactivity of CaO-based sorbent for carbon capture. *Ind. Eng. Chem. Res.* **2013**, *52*, 2241–2246. [[CrossRef](#)]
107. Ma, Z.; Li, Y.; Zhang, W.; Wang, Y.; Zhao, J.; Wang, Z. Energy storage and attrition performance of limestone under fluidization during CaO/CaCO<sub>3</sub> cycles. *Energy* **2020**, *207*, 118291. [[CrossRef](#)]
108. Obermeier, J.; Sakellariou, K.G.; Tsongidis, N.I.; Baciú, D.; Charalambopoulou, G.; Steriotis, T.; Müller, K.; Karagiannakis, G.; Konstandopoulos, A.G.; Stubos, A.; et al. Material development and assessment of an energy storage concept based on the CaO-looping process. *Sol. Energy* **2017**, *150*, 298–309. [[CrossRef](#)]
109. Sarrion, B.; Sanchez-Jimenez, P.E.; Perejon, A.; Perez-Maqueda, L.A.; Valverde, J.M. Pressure Effect on the Multicycle Activity of Natural Carbonates and a Ca/Zr Composite for Energy Storage of Concentrated Solar Power. *ACS Sustain. Chem. Eng.* **2018**, *6*, 7849–7858. [[CrossRef](#)]
110. Li, B.; Li, Y.; Sun, H.; Wang, Y.; Wang, Z. Thermochemical Heat Storage Performance of CaO Pellets Fabricated by Extrusion–Spheronization under Harsh Calcination Conditions. *Energy Fuels* **2020**, *34*, 6462–6473. [[CrossRef](#)]
111. Durán-Martín, J.D.; Jimenez, P.E.S.; Valverde, J.M.; Perejón, A.; Arcenegui-Troya, J.; Triñanes, P.G.; Maqueda, L.A.P. Role of particle size on the multicycle calcium looping activity of limestone for thermochemical energy storage. *J. Adv. Res.* **2020**, *22*, 67–76. [[CrossRef](#)]
112. Prieto, C.; Cooper, P.; Fernández, A.I.; Cabeza, L.F. Review of technology: Thermochemical energy storage for concentrated solar power plants. *Renew. Sustain. Energy Rev.* **2016**, *60*, 909–929. [[CrossRef](#)]
113. Abanades, J.C. The maximum capture efficiency of CO<sub>2</sub> using a carbonation/calcination cycle of CaO/CaCO<sub>3</sub>. *Chem. Eng. J.* **2002**, *90*, 303–306. [[CrossRef](#)]
114. Jiang, L. Comprehensive utilization situation of fly ash in coal-fired power plants and its development suggestions. *Clean Coal Technol.* **2020**, *26*, 31–39.
115. Benitez-Guerrero, M.; Valverde, J.M.; Sanchez-Jimenez, P.E.; Perejon, A.; Perez-Maqueda, L.A. Multicycle activity of natural CaCO<sub>3</sub> minerals for thermochemical energy storage in Concentrated Solar Power plants. *Sol. Energy* **2017**, *153*, 188–199. [[CrossRef](#)]
116. Setoodeh Jahromy, S.; Azam, M.; Jordan, C.; Harasek, M.; Winter, F. The Potential Use of Fly Ash from the Pulp and Paper Industry as Thermochemical Energy and CO<sub>2</sub> Storage Material. *Energies* **2021**, *14*, 3348. [[CrossRef](#)]
117. Perejón, A.; Valverde, J.M.; Miranda-Pizarro, J.; Sánchez-Jiménez, P.E.; Pérez-Maqueda, L.A. Large-Scale Storage of Concentrated Solar Power from Industrial Waste. *ACS Sustain. Chem. Eng.* **2017**, *5*, 2265–2272. [[CrossRef](#)]
118. Valverde, J.M.; Miranda-Pizarro, J.; Perejón, A.; Sánchez-Jiménez, P.E.; Pérez-Maqueda, L.A. Calcium-Looping performance of steel and blast furnace slags for thermochemical energy storage in concentrated solar power plants. *J. CO<sub>2</sub> Util.* **2017**, *22*, 143–154. [[CrossRef](#)]
119. Bai, S.; Zhou, Y.; Chen, Y.; Wang, Z.; Sun, J.; Zhao, C. Thermochemical Energy Storage Performances of Steel Slag-Derived CaO-Based Composites. *Chem. Eng. Technol.* **2020**, *43*, 2190–2197. [[CrossRef](#)]

120. Setoodeh Jahromy, S.; Jordan, C.; Azam, M.; Werner, A.; Harasek, M.; Winter, F. Fly Ash from Municipal Solid Waste Incineration as a Potential Thermochemical Energy Storage Material. *Energy Fuels* **2019**, *33*, 5810–5819. [[CrossRef](#)]
121. Maaten, B.; Konist, A.; Siirde, A. Potential of solid residues from power plants as thermochemical energy storage materials. *J. Therm. Anal. Calorim.* **2020**, *142*, 1799–1805. [[CrossRef](#)]
122. Arcenegui-Troya, J.; Sánchez-Jiménez, P.E.; Perejón, A.; Valverde, J.M.; Chacartegui, R.; Pérez-Maqueda, L.A. Calcium-Looping Performance of Biomineralized CaCO<sub>3</sub> for CO<sub>2</sub> Capture and Thermochemical Energy Storage. *Ind. Eng. Chem. Res.* **2020**, *59*, 12924–12933. [[CrossRef](#)]
123. Scaltsoyiannes, A.A.; Lemonidou, A.A. On the factors affecting the deactivation of limestone under calcium looping conditions: A new comprehensive model. *Chem. Eng. Sci.* **2021**, *243*, 116797. [[CrossRef](#)]
124. Huang, C.-H.; Chang, K.-P.; Yu, C.-T.; Chiang, P.-C.; Wang, C.-F. Development of high-temperature CO<sub>2</sub> sorbents made of CaO-based mesoporous silica. *Chem. Eng. J.* **2010**, *161*, 129–135. [[CrossRef](#)]
125. Sanchez-Jimenez, P.E.; Perez-Maqueda, L.A.; Valverde, J. Nanosilica supported CaO: A regenerable and mechanically hard CO<sub>2</sub> sorbent at Ca-looping conditions. *Appl. Energy* **2014**, *118*, 92–99. [[CrossRef](#)]
126. Benitez-Guerrero, M.; Valverde, J.M.; Perejon, A.; Sanchez-Jimenez, P.E.; Perez-Maqueda, L.A. Low-cost Ca-based composites synthesized by biotemplate method for thermochemical energy storage of concentrated solar power. *Appl. Energy* **2018**, *210*, 108–116. [[CrossRef](#)]
127. Chen, X.; Jin, X.; Liu, Z.; Ling, X.; Wang, Y. Experimental investigation on the CaO/CaCO<sub>3</sub> thermochemical energy storage with SiO<sub>2</sub> doping. *Energy* **2018**, *155*, 128–138. [[CrossRef](#)]
128. Bird, J.E.; Humphries, T.D.; Paskevicius, M.; Poupin, L.; Buckley, C.E. Thermal properties of thermochemical heat storage materials. *Phys. Chem. Chem. Phys.* **2020**, *22*, 4617–4625. [[CrossRef](#)] [[PubMed](#)]
129. Khosa, A.A.; Zhao, C.Y. Heat storage and release performance analysis of CaCO<sub>3</sub>/CaO thermal energy storage system after doping nano silica. *Sol. Energy* **2019**, *188*, 619–630. [[CrossRef](#)]
130. Møller, K.T.; Ibrahim, A.; Buckley, C.E.; Paskevicius, M. Inexpensive thermochemical energy storage utilising additive enhanced limestone. *J. Mater. Chem. A* **2020**, *8*, 9646–9653. [[CrossRef](#)]
131. Benitez-Guerrero, M.; Valverde, J.M.; Sanchez-Jimenez, P.E.; Perejon, A.; Perez-Maqueda, L.A. Calcium-Looping performance of mechanically modified Al<sub>2</sub>O<sub>3</sub>-CaO composites for energy storage and CO<sub>2</sub> capture. *Chem. Eng. J.* **2018**, *334*, 2343–2355. [[CrossRef](#)]
132. Fedunik-Hofman, L.A.; Bayon, A.; Lipinski, W.; Donne, S.W. Investigation of novel hydroxyapatite-doped CaO material for calcination-carbonation thermochemical energy storage. *AIP Conf. Proc.* **2018**, *2033*, 100004.
133. Han, R.; Gao, J.; Wei, S.; Su, Y.; Su, C.; Li, J.; Liu, Q.; Qin, Y. High-performance CaO-based composites synthesized using a space-confined chemical vapor deposition strategy for thermochemical energy storage. *Sol. Energy Mater. Sol. Cells* **2020**, *206*, 110346. [[CrossRef](#)]
134. Sun, H.; Li, Y.; Yan, X.; Zhao, J.; Wang, Z. Thermochemical energy storage performance of Al<sub>2</sub>O<sub>3</sub>/CeO<sub>2</sub> co-doped CaO-based material under high carbonation pressure. *Appl. Energy* **2020**, *263*, 114650. [[CrossRef](#)]
135. Sun, H.; Li, Y.; Yan, X.; Wang, Z.; Liu, W. CaO/CaCO<sub>3</sub> thermochemical heat storage performance of CaO-based micrometre-sized tubular composite. *Energy Convers. Manag.* **2020**, *222*, 113222. [[CrossRef](#)]
136. Møller, K.T.; Humphries, T.D.; Berger, A.; Paskevicius, M.; Buckley, C.E. Thermochemical energy storage system development utilising limestone. *Chem. Eng. J. Adv.* **2021**, *8*, 100168. [[CrossRef](#)]
137. Lu, S.; Wu, S. Calcination-carbonation durability of nano CaCO<sub>3</sub> doped with Li<sub>2</sub>SO<sub>4</sub>. *Chem. Eng. J.* **2016**, *294*, 22–29. [[CrossRef](#)]
138. Khosa, A.A.; Yan, J.; Zhao, C.Y. Investigating the effects of ZnO dopant on the thermodynamic and kinetic properties of CaCO<sub>3</sub>/CaO TCES system. *Energy* **2021**, *215*, 119132. [[CrossRef](#)]
139. Xu, T.; Tian, X.; Khosa, A.; Yan, J.; Ye, Q.; Zhao, C. Reaction performance of CaCO<sub>3</sub>/CaO thermochemical energy storage with TiO<sub>2</sub> dopant and experimental study in a fixed-bed reactor. *Energy* **2021**, *236*, 121451. [[CrossRef](#)]
140. Sánchez Jiménez, P.E.; Perejón, A.; Benítez Guerrero, M.; Valverde, J.M.; Ortiz, C.; Pérez Maqueda, L.A. High-performance and low-cost macroporous calcium oxide based materials for thermochemical energy storage in concentrated solar power plants. *Appl. Energy* **2019**, *235*, 543–552. [[CrossRef](#)]
141. Han, R.; Gao, J.; Wei, S.; Sun, F.; Liu, Q.; Qin, Y. Development of dense Ca-based, Al-stabilized composites with high volumetric energy density for thermochemical energy storage of concentrated solar power. *Energy Convers. Manag.* **2020**, *221*, 113201. [[CrossRef](#)]
142. Han, R.; Gao, J.; Wei, S.; Su, Y.; Sun, F.; Zhao, G.; Qin, Y. Strongly coupled calcium carbonate/antioxidative graphite nanosheets composites with high cycling stability for thermochemical energy storage. *Appl. Energy* **2018**, *231*, 412–422. [[CrossRef](#)]
143. Han, R.; Xing, S.; Wu, X.; Pang, C.; Lu, S.; Su, Y.; Liu, Q.; Song, C.; Gao, J. Compressing Two-Dimensional Graphite-Nanosheet-Supported CaO for Optimizing Porous Structures toward High-Volumetric-Performance Heat Storage. *Energy Fuels* **2021**, *35*, 10841–10849. [[CrossRef](#)]
144. Song, C.; Liu, X.; Zheng, H.; Bao, C.; Teng, L.; Da, Y.; Jiang, F.; Li, C.; Li, Y.; Xuan, Y.; et al. Decomposition kinetics of Al- and Fe-doped calcium carbonate particles with improved solar absorbance and cycle stability. *Chem. Eng. J.* **2021**, *406*, 126282. [[CrossRef](#)]

145. Li, B.; Li, Y.; Dou, Y.; Wang, Y.; Zhao, J.; Wang, T. SiC/Mn co-doped CaO pellets with enhanced optical and thermal properties for calcium looping thermochemical heat storage. *Chem. Eng. J.* **2021**, *423*, 130305. [[CrossRef](#)]
146. Yang, L.; Huang, Z.; Huang, G. Fe- and Mn-Doped Ca-Based Materials for Thermochemical Energy Storage Systems. *Energy Fuels* **2020**, *34*, 11479–11488. [[CrossRef](#)]
147. Zheng, H.; Song, C.; Bao, C.; Liu, X.; Xuan, Y.; Li, Y.; Ding, Y. Dark calcium carbonate particles for simultaneous full-spectrum solar thermal conversion and large-capacity thermochemical energy storage. *Sol. Energy Mater. Sol. Cells* **2020**, *207*, 110364. [[CrossRef](#)]